

Prediction of large events on a dynamical model of a fault

*S. L. Pepke,<sup>◇</sup> J. M. Carlson,<sup>◇\*</sup> and B. E. Shaw,<sup>\*†</sup>*

<sup>◇</sup>Department of Physics, University  
of California, Santa Barbara, CA  
93106

<sup>†</sup> Lamont-Doherty Earth Observatory,  
Columbia University, Palisades, NY  
10964

<sup>\*</sup>Institute for Theoretical Physics,  
University of California, Santa  
Barbara, CA 93106

ABSTRACT: We present results for long term and intermediate term prediction algorithms applied to a simple mechanical model of a fault. We use long term prediction methods based, for example, on the distribution of repeat times between large events to establish a benchmark for predictability in the model. In comparison, intermediate term prediction techniques, analogous to the pattern recognition algorithms CN and M8 introduced and studied by Keilis–Borok et al., are more effective at predicting coming large events. We consider the implications of several different quality functions  $Q$  which can be used to optimize the algorithms with respect to features such as space, time, and magnitude windows, and find that our results are not overly sensitive to variations in these algorithm parameters. We also study the intrinsic uncertainties which are associated with seismicity catalogs of restricted lengths.

## I. Introduction

Prediction of the occurrence of large earthquakes within a narrow space-time window on a fault has proven to be a difficult problem for several reasons: i) time scales over which reliable and detailed seismological records are available are often small compared to recurrence times within a fault zone, ii) complexity of fault geometry and dynamics leads to great variability in premonitory phenomena, iii) initiating mechanisms for large events are not completely understood (which inhibits the determination of the relative importance of various precursors), and iv) knowledge of the strain distribution and yield points along faults is insufficient to indicate the locations of future epicenters. The above make it difficult not only to predict well, but also to determine how inherently predictable the system is and to find optimal forecasting methods.

With relatively little certain knowledge concerning the system, one must be concerned with optimizing prediction using the data at hand as well as objectively evaluating the quality of the predictions that are made. In seismology, these goals cannot be met using seismicity catalogs alone, because they represent only a rather brief record of the system relative to the time scale of the seismic cycle. One possible path forward is through the use of artificial catalogs to compare methods of forecasting, since one may generate a wealth of statistics for them on the computer and also have the ability to vary system parameters.

In this paper we present results for long term and intermediate term prediction algorithms applied to catalogs generated from a dynamical model of a fault. Our objective is not to prove that a particular model will quantitatively duplicate the complex seismicity patterns observed on real faults, though certainly such an outcome would be of great interest. Instead, this study will address issues related to algorithm optimization and the intrinsic limitations of algorithms given the sparsity of data for the earth. We consider long term prediction techniques, such as the time-predictable and slip-predictable algorithms, which are based solely on characteristics of the most recent large event. In a similar spirit, we also make predictions based on the distribution of time intervals between large events, which can be determined to arbitrary accuracy on a model such as that which will be considered here. However, the principle results of this paper involve intermediate term prediction techniques analogous to those which have been developed by *Keilis-Borok et al.* [1990a, b] and have recently been the object of much attention (see, e.g., *Healey, et al.* [1992]). The aim of these algorithms is to provide an objective means for assessing the probabilities of large earthquakes based on a collection of precursor functions, the values of which are determined by regional small and medium size events. The precursor functions include overall activity, rate of change of activity, and clustering of events, and they are evaluated in coarse grained space-time windows. Simple pattern recognition techniques are then used to select the most relevant precursors from a larger set of possibilities and to establish threshold levels for signaling an alert. On the model we consider the simplest versions of these algorithms using only single precursors and find that they do perform better than long term prediction techniques. However, for the most standard precursors, such as the level of seismic activity, the algorithms do not work as well as we had hoped. This still leaves open the possibility that algorithms which utilize a combination of precursors will be more effective. In addition, it is worth noting that one particular precursor function, which is related to the degree to which seismicity extends throughout the region, does significantly outperform the other precursor functions we have considered, and leads to fairly reliable predictions on the time scale which is relevant for intermediate term prediction.

Synthetic catalogs have been used a great deal in the past couple of decades. Usually, they provide a testing ground for algorithms designed for things such as foreshock and aftershock identification, as well as prediction. As far as we know, to date synthetic catalogs have not been used as a means for improving prediction algorithms, despite the

obvious benefits of synthetic catalogs, which include better statistics and well-understood quantified properties. These features allow for algorithm development and the study of optimization procedures to an extent which is not possible for real catalogs. In the face of little theoretical understanding of the problem of prediction in such a complex system as the earth's crust, volumes of literature have been published documenting possible precursory phenomena and event distributions. Yet little is written on how best to use such information. It is with respect to this question of optimal use of available information that synthetic catalogs may prove most useful.

It is important to distinguish the two main types of artificial catalogs, each of which provides a means to a different end. First, there are purely statistical catalogs, which are constructed to satisfy certain statistical constraints, such as consistency with the Gutenberg–Richter law, Omori's law, and/or spatio-temporal clustering. However, because these catalogs are not based on an underlying physical process, as a test for predictability they are most useful to provide lower bounds on the effectiveness of an algorithm. A good algorithm should detect some inherent correlation which has not been put in by hand and, thus, should do better on the earth than it does on any statistically generated catalog.

In contrast, one can consider artificial catalogs generated by dynamical models as we do here. We will use the model-generated catalogs as a means to the end of algorithm optimization, letting the *physical* mechanisms guide us in determining which properties of the catalogs are important for prediction. Here, unlike the purely statistical catalogs, no features are *a priori* built in. Our goal is to identify features which are generic to a class of physical models and discover how those features function in prediction algorithms which may be easily adapted to different fault systems worldwide.

The model which we consider is a one-dimensional homogeneous model for a fault, which has recently been studied in a variety of different contexts including the statistical analysis of intrinsic scaling laws [Carlson, *et al.*, 1991], and applications to dynamical fracture [Langer and Tang, 1991; Langer, 1992]. The model is a particularly good candidate for studies of seismic phenomena because many of its fundamental features are reminiscent of behavior which is observed in the earth. For example, the magnitude vs. frequency distribution is similar to what is observed for a single fault or narrow fault zone [Carlson and Langer, 1989*a, b*], and the model generates a moment spectrum similar to those inferred from seismographic observations [Shaw, 1993*a*]. The model is also a particularly good candidate for studies of predictability because, firstly, it is deterministically chaotic, and hence technically unpredictable at long enough times. Secondly, the model exhibits a sharp distinction between small and large events. The smaller, more numerous events tend to cluster in the neighborhood of an epicenter of a future large event [Shaw *et al.*, 1992]. This local increase in activity is a generic precursor in the model (other precursor functions will also be considered) and is the primary statistical basis for predictability at shorter time scales. While the analogous behavior is much less systematic in the earth [Kanamori, 1981], a similar rise in regional activity has been observed on some occasions prior to large events, and is one of the signals used for prediction in the algorithms such as CN and M8 which were introduced and studied by Keilis–Borok *et al.*, [1990 *a, b*]. The last important feature in the model is its simplicity, which allows us to numerically generate the equivalent of millions of years data with perfect detection of events. This feature allows us to evaluate quantitatively the success of algorithms in a manner that is impossible for real catalogs.

Our model has the additional advantage of requiring no fine-tuning of parameters. In particular, there is a minimal number of input parameters, all of which are physically meaningful, yet with respect to which the qualitative catalog features are robust over a wide range of values. Further, we expect to be able to predict events on the model better

than on the real system, but that is to the point: to establish predictability limits for these nonlinear dynamical models and to optimize on a “clean” system. We hope that the things we learn by doing so will shed light on the roles of various phenomena occurring during the preparatory period for a large event and allow us to distinguish correctly between meaningful causal premonitory characteristics and misleading happenstance trends. Ultimately, the prediction algorithms will be tested on more sophisticated versions of the model which may include aftershocks, a coupled fault geometry, or be embedded in a two-dimensional medium.

The organization of the paper is as follows. In Section II relevant characteristics of the uniform Burridge–Knopoff (UBK) model are reviewed. This includes descriptions of pertinent length and time scales which play a role in the model’s predictability. In Section III we introduce the quality functions  $Q$ , which are the means by which we evaluate the success of the algorithms. In Section IV we present results for long term prediction, including the slip-predictable model, the time-predictable model, and prediction based upon recurrence intervals. Such methods are perhaps the most widely established procedures for determining earthquake probabilities along faults. Section V contains our results for prediction based upon intermediate term precursors. The forecasting method is outlined and applied to individual activity-based precursor functions on the model. Section VI discusses the robustness of our results with respect to variation of the algorithm and catalog parameters, including variations in catalog length. Section VII gives a summary and addresses outstanding problems.

## II. Relevant Model Characteristics

In the finite difference approximation, the model considered here is one of a class first applied to earthquake dynamics by *Burridge and Knopoff* [1967]. It was reintroduced in its simplest form and analyzed in a modern context by *Carlson and Langer* [1989a, b]. The one-dimensional uniform Burridge–Knopoff (UBK) model represents the motion of one side of a lateral fault which is driven by a slow shear deformation relative to the other side of the fault and which is subject to a velocity–weakening slip-stick friction law at the interface. The system consists of  $N$  blocks. Each block is coupled to its nearest neighbors with coil springs representing the linear elastic response of the system to compressional deformations. A leaf spring attaches each block to a fixed upper surface, and represents the linear elastic response of the system to shear deformations. The blocks are constrained to move on the surface of the sliding plate. The system is loaded slowly by moving the lower plate at a velocity  $\nu$  until one of the blocks exceeds the frictional threshold. That block then begins to slide, dissipating energy as determined by the friction law. The initially negative slope of the friction law leads to the essential dynamical instability which maintains the complexity of the series of events over arbitrarily long time periods. An event is considered over when all of the blocks have come to rest.

In the continuum limit the partial differential equation describing slipping motion along the fault is:

$$\ddot{U} = \frac{\partial^2 U}{\partial s^2} - U - \phi[\dot{U} + \nu] \quad (1)$$

where  $U(s, t)$  is the displacement measured with respect to the fixed upper plate as a function of position  $s$  and time  $t$ . Dots denote derivatives with respect to the dimensionless time  $t$ , which has been scaled by the characteristic slip time for a (homogeneous) large event. Displacements  $U$  have been scaled by the corresponding characteristic slip distance. In Eq. (1) lengths  $s$  are measured in units of a stiffness length which is given by the distance a sound wave travels (of order ten kilometers) in the characteristic slip time  $\Delta t = 1$ . In

the finite difference version of (1), the coefficient of the lattice Laplacian is the number of blocks  $\ell$  in this characteristic length, so that the equilibrium block spacing  $1/\ell$  is the small scale cutoff. This parameter plays a role in the dynamics of the UBK model (see, e.g., *Langer and Tang*, [1991]), and recent measurements of microearthquakes suggest that there may be a small scale cutoff in the earth as well. In particular, the measurements of changes in the distribution of sizes of very small events [*Malin, et al.*, 1989; *Aki*, 1987] and measurements which suggest that the smallest earthquakes may have a nearly constant rupture area (see, e.g., *Bakun, et al.* [1976], and *Archuleta et al.* [1982]), lead to a small length cutoff ranging from meters to a few hundred meters. This suggests that in units of the characteristic stiffness length (roughly 10 kilometers as mentioned above) realistic values of  $\ell$  are of order  $10^2 - 10^4$ , i.e. a large number. Here we will take  $\ell = 10$  for numerical convenience. In *Carlson et al.* [1991] the scaling of the UBK model as a function of  $\ell$  was considered. The parameter  $\nu$  in (1) is the dimensionless pulling speed, given by the ratio of the rise time to the loading period between large events. Realistic values of  $\nu$  are thus  $10^{-8}$  or less. Here we will take  $\nu$  to be small enough to preserve the separation of time scales between individual events and the loading mechanism. For technical reasons when we do this we must also introduce the small parameter  $\sigma$  into the velocity-weakening friction law which we will take to be

$$\phi(z) = \begin{cases} (-\infty, 1], & z = 0; \\ (1 - \sigma)/\{1 + [2\alpha z/(1 - \sigma)]\}, & z > 0. \end{cases} \quad (2)$$

Here  $\sigma$  replaces  $\nu$  in setting the scale for the displacement of the smallest events, and we can set  $\nu = 0$  while the blocks slip. The friction parameter  $\alpha$  is the ratio of the characteristic slipping speed to the speed at which the friction is reduced by half the difference between the threshold value and the value it attains at high speeds. It is difficult, if not impossible, to determine realistic values of  $\alpha$  from laboratory measurements. For a wide range of  $\alpha$  the behavior of the UBK model is not particularly sensitive to the exact value. Throughout most of this paper we will take  $\alpha = 3$  which is in this range. As pointed out by *Vasconcelos, et al.* [1992] and in *Carlson, et al.* [1991], for  $\alpha$  small enough the behavior does change substantially, though we believe that this regime is less relevant to seismicity. The results which we present in this paper are relevant in the regime where  $\ell$  is large,  $\sigma$  is small, and  $\alpha$  is large enough to generate the generic behavior. As discussed above, this regime is most relevant for seismological applications.

It is important to note that the UBK model is homogeneous in all of its material properties. We observe complex behavior as a consequence of a dynamical instability associated with the friction law. Beginning with a small heterogeneity in the initial condition, we allow the system to evolve through several loading cycles until it reaches a statistically steady state, at which point the statistical properties are independent of the details of the initial conditions. In Fig. 1 we plot a small fraction (both in space and time) of the catalog which will be used in this paper, which begins after the initial transient period has passed. For each event, a line segment is drawn through all of the blocks that slip, and a cross marks the position of the epicenter for each large event. While there are clear correlations at shorter time scales, because of the underlying homogeneity of the UBK model the long time average of the locations of epicenters of large events is independent of position— an event could happen anywhere with equal probability.

The behavior of this system is found to resemble that of an earthquake fault in several important respects. Defining the seismic moment  $M$  to be the total slip during an event:

$$M = \int_{\text{event}} \delta U(s) ds \quad (3)$$

and the magnitude  $\mu = \ln M$ , we find that for wide ranges of the above parameter values, for small to medium size events the UBK model generates frequency-magnitude distributions described by the Gutenberg–Richter law  $D(\mu) = Ae^{-b\mu}$ . Here  $D(\mu)d\mu$  is the frequency of occurrence of events in the magnitude interval  $[\mu, \mu + d\mu]$  per unit length per unit time (see Fig. 2). As long as  $\alpha$  is sufficiently large ( $\alpha \geq 2.5$ ), we obtain  $b = 1$  robustly in this region. In contrast, the largest events follow a different distribution which indicates an overfrequency of these events relative to the frequency extrapolated from the distribution of small events. The large events are responsible for nearly all of the moment release in the UBK model. The overfrequency implies that there will be a characteristic repeat time between large events, as discussed by *Carlson* [1991], which can be exploited for the purposes of long term prediction. The change in behavior between the small and large events is characterized by the length  $\tilde{\xi} \equiv \frac{2}{\alpha} \ln(\frac{4\ell^2}{\sigma})$ . In *Carlson and Langer* [1989b] it was shown that events which are triggered in regions of size less than  $\tilde{\xi}$  tend to remain localized, that is, the slip pulses which are generated will decay rapidly when they encounter regions which are far from threshold. In contrast, when the initial triggering zone is larger than  $\tilde{\xi}$ , the slip pulses will tend to propagate much further. The length scale  $\tilde{\xi}$  coincides well with the upper bound on the clustering of small events such as those illustrated in Fig. 1, and the associated crossover magnitude  $\tilde{\mu} = \ln(2/\alpha)$  coincides with the minimum in the magnitude vs. frequency distribution (Fig. 2). Roughly speaking, the smaller events smooth the spatial configuration on length scales less than  $\tilde{\xi}$ , thus preparing a region for the triggering of a large roughening event. This pattern leads to spatio-temporal clustering of small scale activity along the fault prior to a large event, as reported by *Shaw, et al.*, [1992]. While this systematic increase in activity is a key feature leading to the relative success of the intermediate term prediction algorithms on the UBK model, this observation alone is not sufficient to determine whether ultimately the UBK model will be more or less predictable than the earth.

Throughout this work we distinguish between “small” premonitory events and the “large” events we wish to forecast. This distinction can be made precisely in the UBK model: small events are taken to be those for which  $\mu < \tilde{\mu}$  while large events have  $\mu \geq \tilde{\mu}$ . While the existence of a sharp feature is useful here to obtain quantitative results, the relatively small number of events of size near  $\tilde{\mu}$  compared to events of lesser or greater magnitude, implies that our results will not depend strongly on the exact criterion for the crossover that is used. This division is certainly much less precise in real data. It is interesting to note that when data from an individual fault or narrow fault zone is considered, as in the UBK model an overfrequency of large events is observed [*Wesnowsky, et al.*, 1983; *Schwartz and Coppersmith*, 1984; *Davison and Scholz*, 1985]. In these cases, typical magnitudes of the large events, and geodetic measurements of the plate rates can be used to estimate the recurrence time interval, and make long term predictions. In comparison, data accumulated over a broad region typically does not show an overfrequency of large events. This is a consequence of the fact that faults of many different sizes contribute to regional seismicity. In this case, recent results by *Pacheco, et al.* [1992] suggest a bend, or change in  $b$ -value reflecting an underfrequency of large events, in the magnitude vs. frequency distribution of California seismicity at roughly magnitude 6, which coincides with estimates of the magnitude of events which just span the full depth of the seismogenic zone. These types of regional seismicity catalogs are typically used in intermediate term prediction algorithms such as CN and M8 outlined in Section V.

Simplifications which are inherent in the UBK model used here are its low dimensionality, single fault dynamics, and lack of aftershocks. Systems of interacting faults and different fault geometries may ultimately prove interesting but would be most effectively represented in the context of a fully two-dimensional elastic medium. Studies of a homo-

geneous two-dimensional model are currently under way. In addition, *Shaw* [1993b] has proposed an aftershock mechanism which if added to the two-dimensional model would lead to additional precursory phenomena. Ultimately, we plan to study modified models in the context of prediction as well.

### III. Evaluation of Forecasting Algorithms

In a spatially extended dynamical system, a prediction typically consists of a projection, based on the current status of the system, of the time and location of a coming event. For example, when a hurricane is detected in the ocean, meteorologists attempt to predict the precise time and location at which the storm will contact the coast. In comparison, the forecasts which are made in seismology are necessarily more primitive and involve much longer time scales. Rather than predicting how far in the future an event is likely to take place, one forecasts the likelihood of an event occurring between now and the end of some alarm period. The time windows for such alarms can range from days for short term predictions which are used to alert the public and emergency rescue crews, to years for intermediate term predictions which are used to set certain guidelines for insurance and the allocation of public resources, and even tens of years for long term predictions which are used to establish regional building codes. In algorithms CN and M8 one signals an alert or *time of increased probability* (TIP) to forecast a large event in a specified region in space and time. The most effective algorithms will not issue TIPs unnecessarily. The TIP begins when the algorithm detects that the system is in a state of readiness, and, in order to minimize the cost associated with signaling an alarm, one must wait as long as possible prior to the event before turning on the alarm.

In this context it is worth noting that there are a couple of technical distinctions between algorithms CN and M8 and the intermediate term prediction algorithms which we will consider here. First, in the intermediate term algorithms it will be our goal to predict the *epicenter* of the large events, since in the UBK model the precursory seismicity is strongly correlated with this location (since the long term algorithms make use of only information associated with the last large event, in that case we will attempt to simply predict the time of the next event, rather than focusing on the location of the epicenter). In algorithms such as CN and M8 the spatial regions which are considered are much larger than the size of the large event so targeting the exact location of the future epicenter is much less relevant (in comparison the optimal spatial regions for the UBK model are comparable, and in fact typically somewhat smaller than the size of the event to be predicted). The second distinction is more significant. That is, in CN and M8 the alarm duration is initially fixed to be a specific time interval, typically five years. After this period has passed, the status of the region is reevaluated, and a decision is made regarding whether or not to extend the alert. In contrast, after each event we reevaluate the status of the alarms, and the average alarm duration is determined by the threshold for signaling an alert. In a model such as the UBK model, where the precursor functions tend to increase monotonically in the neighborhood of the epicenter of a future large event, alarms will typically (but not always) stay on until a large event has occurred. This monotonicity in the UBK model is reminiscent of predictions based on time interval distributions, where it only becomes more likely to have a large event the longer it has been since the last one. The fact that such systematic behavior is not generally seen in the earth does not preclude the use of the UBK model to provide diagnostic tests of prediction techniques. The idea here is to test the same sort of prediction algorithms that are used in seismology on a model in which the basic physical mechanisms leading to the complexity are well understood. Our results will help determine which algorithms provide useful information under controlled circumstances, and thus may ultimately be most successful at predicting events in the earth.



With this in mind we now discuss methods for evaluating the long term and intermediate term prediction algorithms which will be considered in subsequent sections. Forecasting necessarily involves tradeoffs between desired outcomes. On one hand, one would like the TIP to be on for a minimal amount of time, but on the other, one would like it to be on at the time a large event takes place. Another consideration which might come into play is the expense associated with issuing false alarms. In general, the cost of signaling an alert must be balanced against the cost of being unprepared when the event ultimately takes place. While deciding how to make this tradeoff is to a large degree based on public policy rather than mathematics or physics, the decision is essential to algorithm optimization.

The success curve, which is defined to be the fraction of events predicted vs. the fraction of time an alert is on, provides one meaningful way to evaluate an algorithm. Here each point on the success curve corresponds to a different value of the threshold for signaling an alert. Such curves are useful to compare different methods of forecasting and thus will be considered extensively in the remainder of the paper (see, e.g., Figs. 6 and 9). However, in order to *set* the threshold that will ultimately be used, one must define a function on such a curve which will select a particular value of the threshold over the others. One function which is commonly considered in the context of algorithms CN and M8 is called the *success ratio* which is defined at each point on the success curve to be:

$$S = \frac{\text{fraction of large events predicted}}{\text{fraction of time the TIP is on}}. \quad (4)$$

Thus  $S$  specifies the gain relative to purely random prediction, for which  $S = 1$ .

Using  $S$  as a measure of the quality of predictions has some inherent complications, as pointed out by *Molchan* [1991] in the context of some time interval distributions. For example, when the alarm time decreases more rapidly than the number of events predicted, one finds that  $S$  diverges as both the alarm time and the fraction of events predicted approach zero. We often observe this behavior in  $S$  when intermediate term prediction algorithms are applied to the UBK model. Systematic algorithm optimization becomes an ill-defined problem in this case.

To solve this problem, we introduce a quality function  $Q$  which will be used to evaluate the long term and intermediate term prediction algorithms discussed in the following sections. It is worth emphasizing that such functions rate the quality of predictions independent of the specific catalog or algorithm to which they are applied, and thus along with the success curve can provide means by which different algorithms can be successfully compared.

The specific choice of a  $Q$  function is somewhat arbitrary. In fact, we have considered several which are discussed in more detail below. Desired features of the  $Q$  function are (1) it should be as simple as possible, with meaningful parameters, so that policy decisions are easily mapped onto parameter settings, (2) the definition should be flexible enough that alternative considerations can easily be incorporated, (3) it should provide a clear measure of when an algorithm is performing well with respect to some simple base measure such as random prediction or doing nothing, (4) it should avoid the pathological behavior as alarm time goes to zero which we observe in  $S$ , and (5) the definition should be robust to small changes in algorithm parameters so that determining a maximum value of  $Q$  is not an overly delicate procedure.

To satisfy the above criteria, we define the quality function  $Q$  in its most general form to be

$$Q = \sum_{i=1}^N A_i p_i, \quad (5)$$

where the  $A_i$  are constant coefficients. We will consider two versions of  $Q$ , which have similar behavior. In the first  $Q = Q_P$  and the  $p_i$  are the probabilities of a set of outcomes with  $0 \leq p_i \leq 1$ , whereas in the second  $Q = Q_R$  the  $p_i$  are interpreted as rates, measured here relative to the overall rate of large events. From a purely scientific point of view, the probability based function  $Q_P$  is the most standard sort of measure, and except near the extreme values of the  $p_i$ 's its performance is similar to an analogous product based function of the form  $\prod p_i^{\alpha_i}$ . In  $Q_P$  we choose to use a sum rather than a product to preserve the symmetry between using the success or failure rate of a given outcome, i.e.  $p_i \rightarrow (1-p_i)$  and  $A_i \rightarrow -A_i$ , is preserved in  $Q_P$  (adding or subtracting a constant from  $Q$  is irrelevant). In contrast, from a public policy point of view, the rate based function  $Q_R$  is potentially the most useful. Here  $Q_R$  may be interpreted as a cost-benefit function, and the coefficients can be set according to the relative costs of the set of possible outcomes. In this case the linear form of  $Q_R$  is essential, since benefits and costs are typically linear functions; doubling the rate at which events are successfully predicted and doubling the rate at which alarms are issued roughly doubles the benefits and costs, respectively. Linear cost-benefit functions have also been used in algorithms applied to real catalogs [Molchan, 1991]. While for the purposes of this paper, the distinction between  $Q_P$  and  $Q_R$  is primarily a technical point (we will often refer to  $Q$  rather than specifically to  $Q_P$  or  $Q_R$  when results and discussions are equally valid for either of these measures), in applications to the earth and public policy decisions there may be a significant benefit to choosing one of these functions over another.

There are three outcomes which we will incorporate into the  $Q$  functions we will be using: the benefit of a successful alarm, the cost of an unsuccessful alarm, and the cost of maintaining an alarm. In both  $Q_P$  and  $Q_R$  (since the rates are defined relative to the rate of large events) we can define  $p_1$  to be the fraction of large events successfully predicted, and  $p_2$  to be the fraction of the total observation time for which alarms are declared. In  $Q_P$  we define  $p_3$  to be the fraction of the total number of alarms that are issued which turn out to be false, while in  $Q_R$ ,  $p_3$  is defined to be the average number of false alarms issued per large event (a nonlinear function of  $p_1$  and  $p_3$  relates the two different definitions of  $p_3$ ). In each case, the penalty for false alarms is necessary to avoid the same sort of pathological behavior referred to above for the success ratio  $S$  in which the solution to the optimization problem is ill-defined and leads to "flickering" alarms which are alternately turned off and on at very short intervals in space and time.

Finally we consider the coefficients  $A_i$  for the  $Q$  functions represented by Eq. (5). Since multiplying  $Q$  by a constant does not change our ultimate conclusions, we can normalize all the  $A_i$  so that  $A_1 = 1$ . Without loss of generality, then, for  $Q$  linear in the three probabilities or rates that we are concerned with, we can define  $Q$  to be

$$Q = p_1 - |A_2|p_2 - |A_3|p_3 \quad (6)$$

where the coefficient of  $p_1$  is positive, since it is a benefit, and the coefficients of  $p_2$  and  $p_3$  are negative, since they are costs. Taking the optimal values for each of the outcomes (i.e. successful prediction of all of the events  $p_1 = 1$ , with negligible costs  $p_2 = p_3 = 0$ ) we obtain the upper bound  $Q \leq 1$ . Alternatively, if one simply does nothing then  $p_1 = p_2 = p_3 = 0$ , and we obtain  $Q = 0$ . We can thus use the  $Q$ 's to say something interesting about an algorithm: given the costs which have been specified, are there outcomes of the algorithm having  $Q > 0$ ; that is, are there strategies that are *better than doing nothing*?

The relative coefficients  $|A_2|$  and  $|A_3|$  must be specified by the user, and, thus, will typically be different in different applications. The parameter  $|A_3|$  sets a tolerance on the number of false alarms that may occur. The cost of a false alarm will depend upon the action which the alarm prompts. In some cases one might be willing to tolerate

quite a few false alarms, as in for example, the case of short term prediction, where the relative cost of issuing a false alarm is much less than the losses that might be spared by successfully predicting a large earthquake. In comparison, for intermediate term prediction one might have a lesser tolerance for false alarms because of the expense associated with maintaining a state of readiness over extended time periods. In the sections that follow we will consider some of the implications of different choices of this coefficient on, for example, the optimization procedure. In some cases for simplicity we will take  $|A_3| = 1$  (in particular, for  $Q = Q_P$ ), and while we expect that this value is somewhat larger than the value which would be used in practice, we will see in Section V that even this choice is not unreasonable, as it leads to a false alarm rate in the intermediate term algorithms which is comparable to those obtained in algorithms CN and M8.

The coefficient  $|A_2|$  measures the cost of maintaining an alarm. Clearly, as  $|A_2| \rightarrow 0$  the best strategy is to leave the alarm on all the time, in which case  $Q = 1 - |A_2|$ . Similarly, as  $|A_2|$  increases, eventually the best strategy will be to do nothing, in which case  $Q = 0$ . Here we will take  $|A_2| = 1$  so that only algorithms which do not maintain a constant state of alert will have a chance of doing better than doing nothing at all.

Ultimately, the different goals of short term, intermediate term, and long term prediction will play a major role in selecting the appropriate function  $Q$  for a particular use. In the coming sections we will use both the success curve and the  $Q$ 's to evaluate prediction algorithms applied to the UBK model, and compare the effectiveness of these two methods. The success curve yields a more general comparison, showing the full range of behavior as the fraction of time occupied by alarms is varied. Consequently, this measure will be most relevant to assessments of the relative performance of algorithms which are intended to operate on different time scales, such as the long term and intermediate term algorithms which will be considered, where the most appropriate  $Q$ 's would be different in the two cases. However, both the success curve and  $Q$  will provide useful information for comparisons between different intermediate term techniques. In particular,  $Q$  yields information about the optimal time scales associated with different intermediate term measures, and provides the most direct assessment of how well an algorithm might be expected to perform in practice. Finally, we cannot explore questions related to short term predictability, because the associated time scales are not present in the UBK model.

#### IV. Long Term Prediction: Results Based on Recurrence Intervals

Long term prediction methods are used to estimate earthquake hazards on a time scale of order tens of years. The simplest such schemes make use of only the magnitude or time of occurrence of the last large event, and are referred to as the time-predictable and slip-predictable models for hazard assessment [*Shimazaki and Nakata, 1980*]. Various applications of both time-predictable [*Scholz, 1985; Bakun and McEvilly, 1984*] and slip-predictable [*Kiremidjian and Anagnos, 1984*] models to real faults have been made. Historical records and geological information are used to construct plots of accumulated slip as a function of time for a particular fault or fault segment. The analogous plot is constructed for the UBK model in Fig. 3, where the results correspond to the accumulated slip for one representative patch along the fault over a time interval which is long compared to available catalogs for real earthquakes, but short compared to the catalogs which we consider later for the UBK model. Essentially all of the slip is associated with large events, which is a feature that is common to both the UBK model and real faults. In the slip-predictable scenario, the magnitude of the coming large event is correlated with the time since the last large event. Here the basic assumption is that were an event to occur today it would relieve all of the accumulated strain. When this is valid the upper corners of the staircase in Fig. 3 should fall on a line. In contrast, in the time-predictable case, the time interval preceding the coming large event is correlated with the magnitude of the last large event. In this case, the assumption is that there is some roughly constant threshold which the local stresses must achieve before a large event will be triggered, and the system must reaccumulate a slip deficit comparable to that which was relieved in the last large event before the next event will be triggered. If this were valid the lower corners of the staircase in Fig. 3 would fall roughly on a line. The best linear least-squares fit to both models are shown in the figure. Although neither works particularly well, the time-predictable model works somewhat better than the slip-predictable model on this relatively short UBK model catalog.

In order to confirm this more generally, in Fig. 4 we test the (a) time-predictable and (b) slip-predictable models on a much longer artificial catalog. We also test for correlations between (c) the moments of subsequent large events and (d) subsequent time intervals. A strong correlation would be indicated by a heavy concentration of points along a well defined curve. A strict adherence to either the time-predictable or slip-predictable model would lead to a concentration of points along a straight line in (a) or (b) respectively. The errors associated with a linear least squares fit to the data indicate that the strongest correlation is observed in 4a which implies that the time-predictable model works best. In fact, none of the others shows any significant correlation at all. In view of the threshold dynamics which govern the UBK model, it is not surprising that the time-predictable model better approximates the behavior we observe. What is more surprising is that even in this case the correlation is very weak. The fact that the points are broadly scattered even in the best case indicates the weakness of these techniques for prediction, even in a simple model. Significantly, however, for short enough catalogs one may find much better correlation with one of the above long term prediction models than actually exists when a sufficient amount of data has been taken into account. Regarding data from real faults, the case is indeterminate due to the few number of data points available for any individual region, as well as problems associated with accurate slip calculation during an event. (See, for example, *Thatcher, [1984]*.) The most reliable data seems to favor time-predictability, however, and the USGS Working Group on California Earthquake Prediction (WGCEP) incorporates this model into its long-term seismic hazard estimates [*WGCEP, 1988, 1990*].

Another method of long term prediction which has been studied extensively in connection with real earthquakes is the use of probability distributions of recurrence times for

large earthquakes on individual faults or fault segments. These are used extensively by agencies such as the USGS [*WGCEP*, 1988, 1990] to estimate the probability of a large event over some time period, say 30 years, given the time of occurrence of the last large event. The difficulty in this method lies in determining the correct distribution, given the sparsity of data for large events on a given fault. By combining data from many different faults, *Nishenko and Buland* [1987] obtained a reasonably good fit to a lognormal distribution. Others [*McNally and Minster*, 1981] have argued that a Weibull distribution is most appropriate. While it is unlikely that the distribution will ever be known exactly, a better understanding of the constraints would be useful because the hazard assessments often rely on features which are several standard deviations away from the mean repeat time. In fact, *Jackson and Davis* [1989] showed that, given the sparsity of data, and the uncertainty in the recurrence time interval distribution, large deviations can substantially alter the estimates for future earthquake hazards, and in some cases lead to a projected decrease in the earthquake hazard estimate for regions which exhibit a longer than expected gap since the last large event.

By comparison, the corresponding distribution can be determined to essentially arbitrary accuracy for a model such as the UBK model. This was done in the case of a short fault (in which large events spanned the entire system) by *Carlson* [1991]. The corresponding distribution is illustrated in Fig. 5a for the long fault catalog that we consider here. The best fit to Gaussian (restricted to positive time intervals), Weibull, and lognormal distributions are also shown for comparison for the cumulative distribution in Fig. 5b. Both the Gaussian and Weibull fit the distribution reasonably well, however, the Gaussian does slightly better. This is primarily due to the fact that the Gaussian somewhat better approximates the non-negligible weight at very short times in Fig. 5 which arises from temporal correlations between large events in neighboring (and, in fact, slightly overlapping) regions. By comparison the lognormal provides a substantially worse fit. As for real earthquakes, in the case of the UBK model the standard deviation is of order the mean repeat time, with  $\sigma/\bar{T} \approx .36$  for the model. This implies that even if the distribution is known quite well, large uncertainties will be inherent in long term prediction schemes. This is discussed in some detail by *Ward* [1992] in a similar application to a synthetic catalog generated from a segmented fault model. In that case a Weibull fit to the cumulative probability distribution proved superior to a lognormal (Gaussian was not tested), with a width which is roughly a factor of two greater than that found in the UBK model.

In order to quantitatively compare our results for time interval prediction with the corresponding results for the intermediate term prediction algorithms discussed in the next sections, it is useful to evaluate this scheme in terms of the success curve discussed in Section III. In the most conventional method of time interval based prediction, given some presumed distribution and known time since the last large event, the probability of a large event in, say, the next thirty years is estimated [*WGCEP*, 1988, 1990]. In contrast, here we specify a threshold time  $t_0$  since the last large event in a region and turn on an alert, or TIP, in that region once a time  $t_0$  has passed. The TIP is turned off once the large event has occurred. For each value of  $t_0$  we then calculate the fraction of earthquakes predicted and the fraction of time the TIP was on. In Fig. 6 the resultant success curve is shown. The data points correspond to the cumulative results for predictions which are made independently for each local position in space, and may be calculated directly from the distribution of time intervals in Fig. 5a. This represents an upper bound on prediction based on recurrence intervals alone, because it incorporates the most detailed spatial information. In comparison, for the purposes of long term prediction spatial information is lost, resulting in a suppression in the success curve, when the fault is coarse grained in the manner which leads to better and more reliable intermediate term predictions. In particular, the lower dashed curve corresponds to predictions which are made in coarse grained regions of length

$3\tilde{\xi}$ , as used in the intermediate term prediction algorithms to follow. The coarse graining of the fault results in greater weight at very short times in the calculated recurrence interval distribution. This is due to events which break through only a few blocks at the edge of a region, leading one to conclude the whole region is unstressed when, in fact, the probability of its sustaining a large event is still quite high.

The results can also be used to evaluate the functions  $Q$  in Eq. (6). Note that for time interval prediction the alarms are only turned off after an event takes place so that the number of false alarms is zero ( $p_3 = 0$ ). Hence the probability based function  $Q_P$  and the cost-benefit function  $Q_R$  are identical, each given by the difference between the fraction predicted  $p_1$  and the fraction of time the TIP is on  $p_2$ :  $Q = p_1 - p_2$ . In Fig. 7 we plot  $Q$  as a function of  $p_2$ . Note that  $Q$  takes a maximum value of  $Q_{\max} = .46$  (for the local predictions) when the TIP is on roughly 1/3 of the time. This corresponds to a threshold time which is 3/4 of the mean recurrence time. In comparison,  $Q_{\max} = .36$  for the coarse grained fault.

In the next section we will see that the the success curve obtained here falls below the corresponding curves for most of the intermediate term prediction algorithms, indicating that if one is concerned solely with maximization of the percent predicted while maintaining TIPs for a minimal amount of time, then the intermediate term prediction methods perform substantially better than prediction based upon recurrence intervals. This is not surprising, given the breadth of the time interval distribution (Fig. 5) and the clustering of small scale activity prior to large events which we have observed in the UBK model. However, time interval prediction is clearly an improvement over both random prediction and the option of doing nothing at all. As a consequence, we expect that this method ultimately will play a role in the optimal prediction algorithm for the UBK model.

## V. Intermediate Term Prediction: The Pattern Recognition Algorithms

Intermediate term prediction algorithms are used to make earthquake hazard assessments on the time scale of one to five years. Because forecasts are made on relatively short time scales compared to long term prediction, more detailed information about the local state of the system must somehow be deduced. Regional small and medium size events provide one possible probe. If a fault or fault segment is near the threshold for slipping then one might expect that the small scale seismicity would also reflect the fact that the system is close to an instability. This sort of behavior occurs more generally in a wide variety of complex systems. For example, in laboratory fracture experiments, the rate of microcrack production accelerates prior to material failure [Mogi, 1962]. In the UBK model, we have observed an increase in the rate of small to medium size events prior to a large event. However, while a local *increase* in seismicity has been observed prior to some large events, and is in part the basis of some intermediate term forecasts of, for example, the Loma Prieta earthquake [Keilis-Borok *et al.*, 1990c], this behavior is much less systematic in the earth. In fact, in some cases a local decrease in small scale seismicity, or quiescence, is observed prior to a large event [Wyss, 1985], and in others no change in the local rate of seismicity is observed at all [Kanamori, 1981]. Herein lies the difficulty of intermediate term prediction. The complexity of the earth yields many different activity patterns so that it is difficult, perhaps impossible, to look at one specific measure to make intermediate term forecasts worldwide.

For that reason Keilis-Borok *et al.* [1990a, b] have developed pattern recognition algorithms, such as CN and M8, which can be applied to interpret objectively the seismicity patterns in earthquake catalogs. As stated above, the idea is that small scale seismicity should signal a coming large event. In these algorithms as many as 18 different possible

precursory phenomena are considered, and each precursor casts a vote as to whether or not an alarm should be turned on. The hope is that if a large event is not preceded by a signal in a particular precursor, then it might be preceded by a signal in another. Algorithms CN and M8 use seven precursor functions and yield a success ratio (Eq. (4)) of roughly  $S = 4$ . In particular, roughly 80% of events are successfully predicted, when the TIPs are on 20% of the time. In comparison, the value of  $S$  for an individual precursor function is typically of order  $S = 2$  or  $3$ , corresponding to successful predictions of only 40% to 60% when the alarm time is 20%. While these values exceed what one would obtain for purely random prediction  $S = 1$ , alarm times which are a smaller fraction of the seismic cycle would be more useful for intermediate term predictions.

On one hand, algorithms such as CN and M8 are the best candidates for objective means to signal alerts, while on another, they remain somewhat speculative because a systematic evaluation using seismicity data is impaired due to the limited amount of available data. In fact, *Dieterich* (in *Healy et al.* [1992]) has suggested that instead of comparing the success of the algorithm to purely random prediction, one should compare to the success obtained when the TIPs are randomly set but with a bias determined by the local rate of large events, thus building in an element of long term prediction. As we will show, even in the case of single precursor functions the intermediate term algorithms do perform well in comparison to long term prediction methods previously discussed for the UBK model. However, for the most standard precursor functions the performance is still not as good as one might expect, and leads to alarm times which are somewhat longer than desired for intermediate term prediction. There is one exception to this, which we will describe in more detail below. Ultimately we hope to provide an answer to the question of whether in general a systematic improvement of these algorithms is possible for the earth.

Below we outline the pattern recognition algorithms which we will use. While we will not consider algorithms which utilize multiple precursors in this paper, our algorithms are designed to closely mimic the simplest versions of the pattern recognition algorithms such as CN and M8 which have been studied extensively in the context of real earthquakes by *Keilis-Borok et al.* [1990a, b], and in earlier model studies by *Gabrielov et al.* [1990]. The algorithms require precursor functions  $\{f_i(\Delta s, \Delta t)\}$ , where  $f_i(\Delta s, \Delta t)$  is the  $i$ th precursor function, evaluated in the spatial region  $\Delta s$  (these are large overlapping circles for the earth, and overlapping line segments in the one-dimensional UBK model which we will take to be a distance one apart) during a sliding time window  $\Delta t$ . Throughout this section we will take  $\Delta s = 3\tilde{\xi}$  and  $\Delta t/\bar{T} = .36$  (i.e. time windows which are 36% of the mean recurrence interval). In Section VI we will show that the performance of the pattern recognition algorithms employed here are not overly sensitive to these choices.

The statistics which are used to evaluate the success curve and quality functions  $Q$  (see Section III) are compiled individually within each of these spatial regions, and then combined to determine the cumulative result. For each region  $R$ , the events which are considered to be in  $R$  are those events for which the *epicenter* lies in  $R$ . For the UBK model our goal is to predict the epicenter of the large events. The precursory seismicity is strongly correlated with the epicenter of coming large events, and it is this correlation which we expect the pattern recognition algorithms to detect. Thus the fraction of large events which is successfully predicted ( $p_1$  in Eq. (6)) in  $R$  is the fraction of events for which the alarm was on in  $R$  when a large event with epicenter in  $R$  takes place. Similarly, the fraction of time an alarm is on ( $p_2$  in Eq. (6)) is also determined for each region individually, as is the fraction (for  $Q_P$ ) or rate (for  $Q_R$ ) of false alarms ( $p_3$ ). As previously stated, unlike algorithms CN and M8, here we will not specify a fixed alarm time. Instead the status of alarms will be reevaluated after each event. Because our precursor functions tend to increase monotonically prior to a large event, once an alarm is turned on it will tend to

stay on until an event takes place. The average alarm time is determined by the threshold value of the precursor function, and a false alarm will be counted if the alarm is turned off before the region in question has contained the epicenter of a large event. Thus false alarms typically arise in two fashions. For relatively low values of the precursor function thresholds, occasionally an alarm may be turned off then reinstated prior to a large event. Alternatively, a region may experience the typical precursory upswelling of activity, but then be preempted as the epicenter by an event which is triggered in a nearby region (recall that the goal is to predict the epicenter). The pathological flickering behavior, in which alarms are rapidly turned off and on, which for injudicious choices of  $Q$  functions can lead to an apparent maximum in  $Q$  as the alarm time goes to zero, is avoided by including this penalty for false alarms with a reasonable choice of the coefficient  $|A_3|$ .

For algorithms CN and M8, precursor functions take a discrete set of values simply referred to as high, medium, or low. A high value (the threshold level “high” is determined from existing catalogs) casts a vote in the favor of issuing a TIP. In our case, we allow for a continuous distribution of values, and the most effective precursor functions will minimize the overlap between the distribution of values taken near the time of a large event and the set of values taken over all time. Examples of both the distribution of values just prior to a large event and the background distribution averaged over all time is illustrated in Fig. 8 for the activity precursor function  $f_1$ . Here activity is defined to be the total number of small to medium size earthquakes, independent of magnitude, within a space-time window (with the exception of events involving only a single block, which are omitted for convenience).

In Fig. 8 we see that the activity  $f_1$  is typically small. The large spike at  $P(f_1) = 0$  reflects the extended quiescent period which is observed just after a large event in the UBK model. In contrast, the conditional probability of the value of  $f_1$  at the time of a large event  $P(f_1|\text{large event})$  has very little weight at  $f_1 = 0$ , because the neighborhood of the epicenter nearly always exhibits some activity just prior to a large event. In fact, within the specified space-time window and for the parameter values we have taken, the activity before a large event can reach values as high as a few hundred events. From Fig. 8 we see that the average activity just before a large event is roughly  $f_1 = 30$ . At that point we observe a ratio of approximately five between the conditional probability and the background value, suggesting that activity should be a good precursor function.

In addition to (1) activity, we will consider the following precursor functions: (2) rate of change of activity  $f_2$  defined to be the slope of a linear least squares fit to the activity as a function of time within a space-time window, (3) fluctuations in activity  $f_3$  defined to be the root mean square deviation from the linear least squares fit used in (2), and (4) active zone size  $f_4$  defined to be the number of blocks that have slipped within the space-time window, independent of how many times they have slipped. Moment-weighted activity was also examined, but found to differ little from activity. While activity, rate of change of activity, and fluctuations in activity all have direct analogies in seismicity catalogs, the active zone size is more difficult to determine for real earthquakes. We choose to consider it here to broaden our set of possible precursors, and, as we will show below, for the UBK model this precursor function performs particularly well. Note that this is the only precursor function which is set to zero after a large event occurs (zeroing the activity in a similar fashion affects the results very little).

Active zone size is a measure of the extent to which seismicity in a given region is diffuse. It is not simply a size or moment weighted activity measure, nor is it a measure of clustering of events. Instead, it is more directly a measure of the broadening or anticlustering of small to moderate size events, which leads to the development of a nucleation region associated with a coming large event. To measure active zone size in the earth a box



counting algorithm might be used, in which the large spatial regions taken in algorithms CN and M8 would be subdivided into many smaller regions, and the number of these smaller regions containing seismicity at or above a certain level would define the regional active zone size. Of course, in the earth this measure is somewhat more complex due to the variable complexity of fault networks in different regions in the earth. However, properly normalized to account for such differences, it may be worth considering because of the exceptional performance of this measure for the UBK model. Compared to activity (Fig. 8) the signal to background ratio is somewhat greater for active zone size, and is somewhat less for rate of change of activity and fluctuations in activity.

Next we will implement the intermediate term prediction algorithm individually for each of the above precursor functions. As previously mentioned, this involves coarse graining the fault into overlapping line segments of size  $\Delta s = 3\tilde{\xi}$  a distance  $\ell$  apart, and evaluating the precursor functions  $\{f_i(\Delta s, \Delta t)\}$  individually on the subset of small to medium size events ( $\mu \leq \tilde{\mu}$ ) which occurs within each space-time window. For each precursor we vary the threshold level for signaling a TIP, and monitor the resulting fraction of the large events ( $\mu > \tilde{\mu}$ ) successfully predicted as well as the fraction of time TIPs were on. This yields the success curves illustrated in Fig. 9. Note that for each of the precursor functions the algorithm leads to an enhancement over random prediction and a clear improvement over the results obtained in the last section using long term techniques. The activity measure  $f_1$ , which is most easily interpreted seismologically, yields results for the UBK model which are somewhat better than those quoted above for algorithms CN and M8, and is a significant improvement over the results obtained using single precursors on real catalogs. In comparison to  $f_1$ , rate of change of activity  $f_2$  performs somewhat worse, and fluctuations in activity  $f_3$  performs significantly worse. This is not too surprising in light of the fact that in the UBK model the increase in activity is essentially monotonic. What is more surprising is the extent to which active zone size  $f_4$  outperforms the others. In that case nearly all of the events are successfully predicted when the alarms are on only 5% of the time. Of those we have considered, active zone size is the only measure which clearly leads to predictions which are relevant on the time scales associated with intermediate term prediction (of order 5% of the recurrence interval).

The corresponding  $Q$  curves for both  $Q_P$  and  $Q_R$  are illustrated in Fig. 10, where it is clear that the results obtained are comparable for the two measures. According to these criteria, the active zone size provides the highest quality (maximum  $Q_{\max}$ ) prediction in both cases. In the UBK model the effectiveness of  $f_4$  as a precursor can be traced to the fact that most of the energy dissipation occurs during large events. In comparison, small to moderate size events relieve relatively little stress. Thus when a small event has occurred it is a direct signal that the blocks involved are poised at the threshold of instability. For a given region, therefore, the active zone size is a more direct measure of the density of blocks that are close to threshold than activity, although these two quantities are clearly related. The second highest quality predictor (for this choice of space-time windows) is the activity, which, in fact, outperforms active zone size for larger alarm time fractions. Because it is most closely related to quantities which are easily calculated from seismicity catalogs, in the next section we will use activity as a base measure with respect to which we will optimize the algorithm. In Fig. 10a for activity, based on the measure  $Q_P$  with  $|A_3| = 1$ , we find that  $Q_{\max}$  occurs when the threshold value  $F_1 = 12$  is used. In this case,  $p_1 = .92$  is the fraction of large events successfully predicted,  $p_2 = .14$  is the fraction of time the alarm is on,  $p_3 = .48$  is fraction of false alarms (i.e. roughly 1/2 of all alarms that are issued do not result in an epicenter of a large event occurring in the region during the associated alarm time). It is interesting to note that the threshold value  $F_1 = 12$  does not coincide with the maximum in the conditional probability illustrated in Fig. 8 indicating room for improvement when ultimately multiple predictors are considered. Finally, using this

criterion for evaluating predictions, rate of change of activity performs somewhat worse, achieving a broad, but low maximum when alarms occupy roughly fifteen percent of the total time, but still provides a significant improvement over doing nothing. In contrast, fluctuations in activity perform significantly worse.

It remains a topic of current research to determine the extent to which our results might be improved by combining the different precursors. For example, appropriate combinations of the precursor functions may lead to threshold functions which result in an increase of the number of successful predictions or a reduction in the false alarm rate and the amount of time occupied by alarms. This is illustrated in Fig. 11, where each point corresponds to the simultaneous measurement of the activity  $f_1$  and the rate of change of activity  $f_2$  (a) over all time and (b) just before a large event. Currently, for activity alone  $Q_P$  is optimized when alarms are declared for activity at or above the threshold level  $F_1 = 12$ . Similarly, for rate of change of activity alone at  $Q_P = Q_{max}$  alarms are declared at or above the threshold level  $F_2 = 120$ . At these values of  $F_1$  and  $F_2$  the set of events which are predicted using  $f_2$  is a subset of those which are predicted using  $f_1$ . However, by comparing the background and conditional distributions, it is clear that in some cases while  $f_1$  maintains a relatively high value,  $f_2$  has dropped far below the value it takes at the time of a large event. Thus by choosing a threshold function such that alarms are declared, for example, only when the values of *both* activity and rate of change of activity exceed some specified individual thresholds one might find that the number of false alarms and the total alarm time could be significantly reduced while the number of successfully predicted events might decrease very little. Such combinations may improve the overall performance in terms of  $Q$ . We are currently developing multidimensional optimization techniques with which we may address this problem in more detail and we hope the results will be useful for further evaluation of the pattern recognition algorithms CN and M8.

## VI. Intermediate Term Prediction: Variation of Parameters

The problem of pattern recognition leads naturally to a question of optimization: under what circumstances is the algorithm most likely to correctly recognize a sequence of events indicating an imminent earthquake? In the most general case, one might consider optimization within the space of all possible algorithms, which make use of an arbitrarily large number of physical attributes (e.g. precursors), and then also optimizing each algorithm with respect to the input parameters which are used. Clearly, this is an extremely high dimensional and difficult problem, which, if feasible, would be of great interest.

In the pattern recognition algorithms such as CN and M8, the basic features of the voting algorithm are fixed, and the problem of pattern recognition refers to the selection of a subset of precursor functions out of a specified list of possibilities as well as optimization with respect to algorithm parameters, such as threshold levels for individual precursor functions. Thus, to make the optimization problem more tractable, the dimensionality of the space is reduced by first deciding on a voting algorithm, and then using specific knowledge of the earthquake process to select possible precursor functions, such as those considered in Section V, which are thought to be most relevant. In this reduced space, the algorithms may be optimized with respect to the remaining parameters.

In a similar manner, in this section we consider the question of optimizing the algorithm studied in Section V for the UBK model. Unless explicitly stated otherwise, we will restrict our attention to the probability based function  $Q = Q_P$ , though some issues related to the sensitivity of certain aspects of the optimization procedure to the choice of  $Q$  functions will also be addressed. The question of restricted magnitude windows will also be considered. In particular, we maximize  $Q(F_i, \Delta s, \Delta t, \Delta \mu)$ , where  $F_i$  is the alarm threshold for the  $i$ th

precursor function  $f_i(\Delta s, \Delta t)$ ,  $\Delta s$  and  $\Delta t$  are the space and time windows within which the function  $f_i$  is evaluated, and  $\Delta\mu$  is the magnitude window from which events are taken. Finally, we consider stability of the maximization procedure as a function of catalog length.

Although the four parameter optimization problem for  $Q(F_i, \Delta s, \Delta t, \Delta\mu)$  is certainly doable in a brute force fashion (the computing resources needed for such a calculation are not too large), it seems sensible to maximize  $Q$  with respect to  $F_i$ ,  $\Delta s$ , and  $\Delta t$  simultaneously in order to first optimize the space and time windows. Then the variation of  $Q_{\max}$  with  $\Delta\mu$  (once again allowing  $F_i$  to vary) may be studied separately. Examining such cross-sections allows for the future possibility of including the magnitude dependence explicitly within the precursor function definitions, as is done in CN and M8.

Below we will restrict our attention to the activity precursor  $f_1$ , because it is the most easily interpreted seismologically.

### *VI.a Optimization with respect to space and time window size*

The pattern recognition algorithms CN and M8 are typically evaluated with time windows of order five years and spatial windows of order one thousand kilometers (the specific size scales with the moment of the large event). Once a TIP is alerted within a particular space-time window, the system is sometimes reevaluated within the original window but on a more finely coarse grained catalog in space (roughly a few hundred kilometers) and time (roughly one year). While these secondary predictions are somewhat less reliable, and do not work well when applied independently, on occasion they do serve to more closely pinpoint the target region for a coming large event.

One interesting, and somewhat surprising feature of CN and M8 is the effectiveness of the large spatial window sizes that are used for the primary predictions. In particular, spatial boxes are typically set to be an order of magnitude larger than the target event. The notion that correlations might extend over anomalously broad regions is akin to the ideas of self-organized criticality introduced by *Bak, Tang, and Wiesenfeld* [1987], which postulate that a large class of driven dissipative systems may be attracted to dynamical states which display large correlations reminiscent of equilibrium critical points, and that this behavior arises due to instabilities associated with threshold dynamics. Such long-range correlations are typically indicated by power law frequency spectra, such as that embodied in the Gutenberg-Richter law describing fault systems. However, because statistics associated with individual faults or narrow fault zones do not exhibit power law behavior over the whole frequency–magnitude spectrum (instead one observes an over-frequency of large events relative to small and medium-sized ones), we do not anticipate that individual faults should be described within the context of a simple critical phenomena theory. It is also for this reason that we would not expect the UBK model to exhibit correlations on scales as large as those used in CN and M8.

In Fig. 12 we evaluate  $Q_{\max}(\Delta s, \Delta t, \Delta\mu)$  for the activity precursor function  $f_1(\Delta s, \Delta t)$  as a function of the spatial  $\Delta s$  and temporal  $\Delta t$  window size. For each data point, the optimization with respect to threshold level  $F_1$  has already been performed, and we include all of the small and medium size events  $\mu_{\min} \leq \mu \leq \tilde{\mu}$ , so that  $\Delta\mu = \tilde{\mu} - \mu_{\min}$  with  $\mu_{\min}$  fixed at the minimum magnitude of a two-block event (the smallest event we have retained in the UBK model catalog), in our evaluation of the activity. The fact that the surface contains a relatively broad maximum, with no sharp features, is an indication that the algorithm is reasonably robust with respect to variations in the parameters. The fact that the maximum is roughly L-shaped indicates that as long as either the spatial windows or the time windows are taken to be near the optimal size, there is reduced sensitivity to variations in the other parameter. We find that the optimal setting is  $\Delta s \approx 3\tilde{\xi}$  and  $\Delta t/\bar{T} \approx .36$ . For these space-time windows, the optimal activity threshold value is  $F_1 = 12$ ,

which leads to a value of  $p_1 = .92$  for the fraction of events successfully predicted, with alarms on  $p_2 = .14$  of the time, and a  $p_3 = .48$  rate of false alarms (i.e. roughly one false alarm for every successful alarm). The value of  $Q_{\max}$  is thus  $Q_{\max} = .30$ .

The natural spatial scale for correlations in the UBK model is  $\tilde{\xi}$ , so it is not surprising that the optimal box size is of order this length. Indeed taking boxes of size  $\tilde{\xi}$  and counting the number of events per box (a box centered at each block) in the time interval preceding a large event, it is found that the box with maximal precursory activity lies within  $\tilde{\xi}/2$  of the future epicenter 80% of the time. Fig. 13a illustrates a slice of an optimization surface (Fig. 12) along the spatial direction. It is clear that  $Q$  rises dramatically up to a length close to  $\tilde{\xi}$  then becomes relatively less sensitive beyond that length. As discussed in more detail below, the coefficient  $|A_3|$  for the false alarm penalty in  $Q$  plays an important role in setting the tolerance for the minimum window size for which reasonable values of  $Q$  are obtained.

Another length scale which is relevant to the problem of spatial optimization is the typical size of a large event  $\xi^*$ . While we do not yet have an analytical expression for  $\xi^*$ , in *Carlson et al.* [1991] numerical simulations were used to deduce that  $\xi^* \sim \ell\tilde{\xi}$ . Thus for the choice of parameters considered here we estimate that  $\xi^* \approx 10\tilde{\xi}$ . While naively one might then expect the algorithm to optimize at  $\xi^*$  we observe a broad peak in  $Q_{\max}$  (see Fig. 13a) at spatial windows between  $3\tilde{\xi}$  and  $4\tilde{\xi}$ . The fact that this is somewhat less than  $\xi^*$  reflects the increased alarm time for larger window sizes, which, because activity is only correlated with an epicenter on length scales of order  $\tilde{\xi}$ , does not result in an increased prediction of epicenters. Thus it is somewhat better to use spatial windows which are smaller than  $\xi^*$  on the UBK model fault. By comparison this spatial window size is significantly smaller than that used in CN and M8.

The optimal time window of  $\Delta t/\bar{T} = .36$  is relatively large, corresponding to time windows which are 36% of the mean recurrence interval. One can see this in Fig. 13b which illustrates a typical slice of the optimization surface (Fig. 12) taken along the temporal direction. As observed previously in *Shaw, et al.* [1992], there is a significant increase in the rate of change of the cumulative activity after on average 2/3 of the cycle time has passed. Because the activity increase is essentially monotonic, and because we have made the alarm time independent of the time window size, there is no cost for having large time windows. As a result the optimization over time windows is essentially picking out the activity “turn-on” time. Note that the optimal time window is relatively much longer than those employed in algorithms CN and M8 (typically 6 years).

The optimal spatial and temporal windows for a few other values of the UBK model parameters were also evaluated (specifically  $l = 10, \alpha = 2$  and  $l = 8, 16, \alpha = 3$ ) and found to be consistent with the above results when expressed in terms of the length  $\tilde{\xi}$  (calculated using the relevant  $l$  and  $\alpha$  values) and the mean repeat time.

Finally, it is worth emphasizing that the large spatial and temporal windows which are selected by our optimization procedure were not obtained when we first attempted to optimize the algorithm with respect to the success ratio (Eq. (4)) or a  $Q$  function which neglects the penalty for false alarms ( $A_3 = 0$  in Eq. (6)). Instead, for example, in the case of the success ratio  $S$  as the space-time windows were decreased  $S$  was found to increase essentially without bound. The analog of this behavior for the  $Q$  which neglects false alarms is illustrated in Figs. 13a and 13b. As previously mentioned, this occurs because as the activity threshold is increased, the alarm time goes to zero faster than the fraction of events successfully predicted, leading to an ill-defined optimization problem.

The incorporation of a penalty for false alarms leads to large space-time windows, and greater reliability of the results. However, it is worth noting that the optimal window size is somewhat sensitive to the choice of the coefficient  $|A_3|$  in  $Q$  (Eq. (6)). For example, in  $Q_P$  we find that the onset of the rapid decrease in  $Q_{\max}$  as the spatial window size is reduced (Fig. 13a) occurs for windows which scale linearly with  $|A_3|$ :  $\Delta s \sim 2|A_3|\tilde{\xi}$ . Thus while for large enough space-time window sizes, the value of  $Q_{\max}$  is generally not very sensitive to the size of the windows, the optimization procedure may lead to smaller windows as the penalty for false alarms is decreased. In fact, in Fig. 13a with the choice  $|A_3| = 1/3$ , the optimal window size is less than  $\tilde{\xi}$ , which results in preemptive false alarms being issued within the nucleating region (of roughly size  $\tilde{\xi}$ ) of the coming large event, simply because the windows were not taken to be large enough (i.e. the active window did not receive credit for predicting the event since it was too small to contain the epicenter). For this reason  $|A_3|$  of order unity is a natural choice for the probability based  $Q_P$ . Furthermore, while qualitatively similar behavior (lack of strong sensitivity of  $Q_{\max}$  over some reasonable range of window sizes, with a cutoff which scales linearly with the false alarm penalty  $|A_3|$ ) is observed for the rate based cost-benefit function  $Q_R$ , the natural choice for  $|A_3|$  in that case will be less because in that case  $p_3$  is a rate (and can thus exceed unity) rather than a probability. For  $Q_R$  we observe that the onset of rapid decay in  $Q_{\max}$  as a function of decreasing  $\Delta s$  scales roughly as  $\Delta s \sim 10|A_3|\tilde{\xi}$ .

### VI.b Magnitude windows

Next we consider the effect of restricting the range of magnitudes which is used to evaluate the activity precursor function. Restricted magnitude windows are an important consideration in seismology because typically reliable data is only available over a relatively narrow range of magnitudes. Furthermore, in CN and M8 seismicity from different magnitude ranges is counted separately as different precursor functions. Because they are more frequent, small events have much more reliable statistics. However, they also tend to swamp the medium sized events in measures such as total activity. By considering only events larger than specified cutoff magnitude we determine whether there is a statistically significant increase in the moderate size events, apart from that predicted by an extrapolation of the increased rate of smaller events which occurs as precursory phenomena. An increased rate of medium size events prior to a large earthquake has been observed in certain instances in the earth (see, e.g., *Pacheo et al.*, [1992]).

In Fig. 14 we illustrate our results for  $Q_{\max}$  as a function of the lower magnitude cutoff  $\mu_{\min}$ . In each case, we use the spatial and temporal windows sizes  $\Delta s = 3\tilde{\xi}$  and  $\Delta t/\bar{T} = .18$ . In addition, the upper cutoff  $\mu_{\max} = \tilde{\mu}$  is fixed. Variations in  $\mu_{\max}$  should not significantly alter the results, because the total activity is dominated by the events at the lower cutoff. From Fig. 14 it is clear that for a wide range of smaller values of  $\mu_{\min}$ ,  $Q_{\max}$  is quite insensitive to the lower magnitude cutoff. In fact, in previous sections we have used this feature to ignore the numerous one-block events in our catalog. These events are the most numerous, but their retention does not improve our results. In contrast, for large values of  $\mu_{\min}$  there is eventually a sharp (linear) decline in  $Q_{\max}$ , which is dominated by a decrease in the number of large events predicted ( $p_1$  in Eq. (6)). It is clear that eventually a decline must be observed once the rate of small to moderate events that will be counted becomes comparable to the overall rate of large events (see Fig. (2)). This corresponds to  $\mu = -7.2$  for the parameters we have chosen. The onset of this behavior occurs for a slightly smaller, but comparable, magnitude  $\mu_{\min} = -7.5$  (the discrepancy is associated with the fact that the algorithm is not generally optimized by setting the threshold at the peak of activity distributions such as Fig. 8). This coincides with a threshold of unity for signaling a TIP. There appears to be a slight maximum in  $Q_{\max}$  just prior to the decline. This suggests that in the UBK model there may be some additional precursory feature associated with

medium size events, and that it may be useful to consider the moderate size events as a precursor separate from the small events as is done in algorithms CN and M8. This feature is more pronounced for time windows which are smaller than the optimal windows for the activity precursor (the figure shows our results for  $\Delta t/\overline{T} = .18$  rather than the window  $\Delta t/\overline{T} = .36$  for optimization with respect to activity for this reason) which reflects the fact that the largest precursory event also typically occurs relatively close in time to the main event.

### *VI.c Variation of catalog length*

Finally we consider the effects of varying the length of the catalog. Because real seismicity catalogs are short compared to the time scale of the seismic cycle (30 years of reliable data on small to moderate size events while the cycle time is of order hundreds of years), restrictions on catalog length may significantly constrain the ability of any seismicity based algorithms to predict. In particular, in order to use pattern recognition algorithms such as those discussed here to predict the most damaging earthquakes, one must be able to use catalogs taken from different fault regions for algorithm selection and optimization. Statistics for several large event cycles are needed to gain reliable information about the conditional probability distributions of precursor function values which may indicate an imminent rupture. Recent local catalogs usually contain only one large event so that the utility of combining many short catalogs in an attempt to reproduce the longer term statistics becomes an important question.

In employing algorithm M8, Keilis-Borok and Kossobokov make the assumption that several extremely short catalogs are nearly as good as one very long catalog when it comes to determining an algorithm for forward prediction of large events. There is really no way to test this hypothesis well on real catalogs due to the lack of availability of catalogs of sufficient length. For the M8 algorithm Keilis-Borok and Kossobokov set the parameters of their algorithm (using eighteen possible precursor functions) to catalogs covering over one hundred earthquakes of magnitude greater than or equal to 8.0. This fitting selects seven of the precursors as most relevant and assigns them discrete threshold values. Using these parameters the algorithm is then applied to 44 additional catalogs from around the world containing large earthquake epicenters. A relevant concern is whether information on even one hundred large event cycles is sufficient to reliably indicate seven out of eighteen functions as viable precursors and assign them appropriate threshold values. Furthermore, in the data fitting procedure, each function threshold is evaluated individually, then these values are retained when precursor functions are combined. Thus it is useful to consider how many large event cycles are needed in each contiguous catalog to select reasonable threshold values for individual precursors, and hence assure the robustness of the results when used for forward prediction.

Another way to phrase the problem is in terms of the ergodicity of the seismological record. The assumption is that averaging over many different earthquake fault realizations in space is equivalent to averaging over a single fault for a much longer time. For the UBK model this reduces to a problem of comparing algorithm selection based upon many short-time catalogs with that obtained at longer times. Since the UBK model is deterministically chaotic, it is not too surprising that we observe ergodic behavior. The interesting question is what minimum catalog length (in terms of large event cycle times) is needed for this ergodic hypothesis to be useful? If the minimum length were much longer than a single cycle time, one could not hope to gain reliable predictability from any number of catalogs containing less than one cycle's worth of data.

In order to examine this problem for our system, we consider the distribution  $P_T(Q, F_1)$  of values of  $Q$  as a function of the threshold  $F_1$  for an ensemble of  $n$  catalogs as the length  $T$

of each of the catalogs is varied. For each catalog length, we choose  $F_1$  in order to maximize the average  $Q$ , defined to be  $\overline{Q}_{\max}$ , and then for that value of  $F_1$  we also compute the fluctuations:  $\sigma^2(Q) = (1/n) \sum_{i=1}^n (Q_i^2 - \overline{Q}_{\max}^2)$ . In order for optimization of the algorithm over many short catalogs to be a useful procedure one must have available catalogs which are sufficiently long that, at a minimum,  $\overline{Q}_{\max}$  attains an acceptable value and, further, the width  $\sigma(Q)$  of the distribution is relatively small. Otherwise, there would be no reason to believe that an algorithm developed, for instance, using current California earthquake catalogs would perform similarly in an independent test either on other catalogs or for forward prediction. Here, for convenience, we will set the spatial  $\Delta s$  window to coincide with the optimal value determined earlier in this section while we take  $\Delta t/\overline{T} = .18$ , which allows for greater range in the catalog lengths which can be compared. We compute the distribution  $P_T(Q, F_1)$  by taking a single extremely long catalog (1848 large event cycles) and breaking it down into groups of sequential catalogs of shorter length ranging from the time window size to several large event cycles.

Figure 15 illustrates our results for the maximized mean value  $\overline{Q}_{\max}$ , as well as the standard deviation  $\sigma(Q)$  as a function of catalog length  $T$  normalized by the mean large event cycle time  $\overline{T}$ . The behavior of  $\overline{Q}_{\max}(T/\overline{T})$  indicates that predictability on the UBK model is poor overall until each short catalog on average encompasses one large event cycle. At this point  $\sigma(Q)$  appears to decrease much less rapidly as well. Only minimal improvements are obtained beyond a single large event cycle time (note that because the fault is sufficiently long that large events do not encompass the entire system, a catalog which extends for one cycle time will typically contain several large events).

For this single predictor, the optimization after one cycle time turns out to be a relatively simple one. In order for a longer catalog on an individual fault to provide information which is not available from combining many shorter time records, the algorithm must make use of correlations which develop on longer time scales. The fact that the fluctuations in  $Q$  for the activity precursor die down on the time scale of a single cycle implies that the activity measure does not contain appreciable information which is relevant on time scales longer than the time scale over which activity builds prior to a large event. Hence, one large event cycle is as good as another for optimization with respect to activity alone and this leads to the rapid decrease in fluctuations in  $\overline{Q}_{\max}$  once most of the catalogs contain at least one large event cycle. We suspect it is the same for the other activity-based precursor functions considered in Section V. If such relatively short time correlations are dominant for seismicity on real faults, then it is not too surprising that the pattern recognition algorithms such as M8 may lead to some measurable enhancement over random prediction and long term techniques. On the other hand, a full cycle's worth of data still corresponds to a much longer catalog than is available for most regions of the earth. Thus an improvement in the stability of algorithms may still occur as the catalogs lengthen— especially in regions with long repeat times.

In addition to ergodicity, the M8 algorithm assumes self-similarity between faults in different regions so that adjusting for the overall seismicity in an area should be sufficient to allow transfer of an algorithm from one fault to another. The question of self-similarity relates most closely to the variation of model parameters. While we have not yet addressed this issue in great detail, as stated previously it appears that optimization is primarily sensitive to the UBK model parameters  $\ell$  and  $\alpha$  through their determination of the length scale  $\tilde{\xi}$  and the shape of the main events peak (for  $\alpha$  and  $\ell$  sufficiently large). These can be adjusted for by variation of the time and space windows utilized for prediction, and hence we expect will present no great obstacle to combining UBK model catalogs once these are set appropriately.

## VII. Conclusions

We have shown how seismicity catalogs generated from a simple deterministic model of an earthquake fault can provide insights into the problem of prediction. The ample statistics available allow for a thorough study of both long and intermediate term methods. We find that while long term prediction based on recurrence intervals performs reasonably well on the time scales that are relevant for long term assessments, these methods are intrinsically limited in effectiveness by the breadth of the distribution of recurrence times. In comparison, intermediate term prediction techniques analogous to algorithms CN and M8 do perform better (especially when the success curve is taken to be the measure of performance) even when they are limited to individual activity based precursor functions. In addition, by optimizing with respect to algorithm parameters, we find that these algorithms do recognize certain fundamental length and time scales in the UBK model. Perhaps most importantly, at least for the simple activity precursor function, the algorithm is as adequately optimized on many relatively short catalogs (in which the length is approximately equal to the mean repeat time) as it is on one longer catalog (containing over 1800 large events). While current catalogs rarely contain a full cycle's worth of data, it is interesting to note that one cycle time rather than many sets the scale for the stability of the algorithm for forward prediction. This result suggests that predictions based on algorithms such as CN and M8 may improve over time as the available catalogs become longer, and while, based on the results of the model, the time scale over which improvements might be expected is certainly appreciable (of order the seismic cycle) our results do suggest that one need not wait forever to obtain substantial gains.

However, on a more pessimistic note, using the most standard measure of seismicity—the overall activity (with or without restricted magnitude windows)—the intermediate term prediction algorithms studied here do not lead to predictions which are as precise as we had hoped. In particular, relative to the cycle time, the alarm time is still much too large: of order 10-20% rather than the 1-5% which is desired. Perhaps these results will improve when multiple precursors are considered. In addition, we did find that one particular measure—the active zone size—did perform measurably better than the rest, capturing nearly all of the large events with roughly a 5% alarm time. However, it is not clear whether any such seismicity based precursor (or combinations of precursors) can perform this well in the earth. Ultimately the kinds of precursors functions which are used in the pattern recognition algorithms may be too primitive to detect correlations on time scales which are desired for relatively precise intermediate term alerts.

Below we summarize additional aspects of the results presented in this paper.

*The quality function  $Q$ :*

One methodological question we have addressed is the evaluation of the performance of a prediction algorithm. For this purpose we have employed two closely related functions  $Q_P$  and  $Q_R$  which exhibit qualitatively similar behavior. The function  $Q_P$  is a linear combination of probabilities relevant to the prediction problem (reflecting the average success rate of prediction, typical alarm times, and the false alarm rate) and was used here to examine optimization questions in some detail. The function  $Q_R$ , on the other hand, is reminiscent of those traditionally employed in cost-benefit analysis and has particularly transparent properties which enable one to determine the public utility of any algorithm. Both  $Q_P$  and  $Q_R$  measure the extent to which an algorithm is able to fulfill all of the prediction goals ( $Q = 1$ ) relative to the option of doing nothing at all ( $Q = 0$ ). This rather simple specification is one which we believe will allow organizations such as public policy committees to more easily determine when it will be in their interest to utilize a prediction algorithm for declaring earthquake alerts.



*Long term prediction:*

We evaluated long term predictability for three commonly used methods: the time-predictable and slip-predictable models as well as prediction based upon recurrence intervals. The results for the time-predictable and slip-predictable models show that neither describes the UBK fault behavior adequately, although the time-predictable case does appear slightly better. It is interesting to note that for either model it is possible to find good correlation over just a few subsequent large events. At any point, however, such a short-time “pattern” could be broken, with the next event differing dramatically from the proposed model. Hence these sorts of models are certainly not sufficient when used alone for prediction on the UBK model fault. This is significant for time-predictable models applied to real faults where positive correlation is often based on knowledge of only two or three events in a given fault region.

Prediction based upon recurrence intervals of large events was examined using the  $Q$  function. At all times this strategy is better than doing nothing because there are no false alarms in the way we have chosen to implement it for the UBK model. Clearly this is not the case for the earth, where, for instance, the more complicated geometry allows the accumulated strain to be relieved along neighboring interacting faults which may not have previously hosted such a large event. The distribution of recurrence times is found to be fit reasonably well by a Gaussian, with comparable results using a Weibull distribution. While neither provides an exact fit, they are both significantly better than a lognormal distribution. This is due to the greater weight at short times seen in the UBK model. In each fit the standard deviation is found to be of order the mean repeat time and the ratio of  $\sigma/\bar{T} \sim 0.36$ , which lies between the ratio of  $\sigma/\bar{T} \sim 0.75$  obtained by *Ward* [1992] for a different model and the intrinsic spread of  $\sigma/\bar{T} \sim 0.21$  proposed by *Nishenko and Buland*, [1987] based on sparse data from real faults. In fact our results are comparable to the value of  $\sigma/\bar{T} \sim .4$  which was ultimately used in the it WGCEP, [1988,1990] forecasts, though there the amount in excess of .21 was ascribed to limited observations rather than intrinsic spread as in the case of the UBK model.

*Intermediate term prediction:*

Intermediate term precursor functions were studied using a pattern recognition technique similar to those introduced and studied by *Keilis-Borok et al.*, [1990a, b]. As indicated above, these methods do outperform long term prediction based on recurrence intervals. When the results for different intermediate term precursors are compared using the  $Q$  functions it is found that  $Q > 0$  when active zone size, activity, and activity rate of change are each employed as individual precursors. Not surprisingly, individually precursors are much more effective at predicting events on the UBK model than in the earth, and, in particular, the active zone size precursor, which in the earth is analogous to the extent to which seismicity is broadly distributed in space, performs remarkably well. For this function, as well as activity and rate of change of activity, the results we obtain are comparable and sometimes better, both in terms of the success curve and the value of  $Q_{\max}$ , than those obtained using the M8 algorithm which employs multiple precursors on real seismicity data.

However, on the UBK model fault, activity is a fairly direct indicator of the approach to the instability which generates the large events, so we had originally expected even better quantitative results. In fact, although we are in the process of examining functions of multiple precursors, it is not obvious that these changes will improve the results substantially. While we suspect that because of its simplicity and the rise in activity which clearly precedes almost every large event, the UBK model will ultimately be more amenable to prediction than will the earth, this need not *a priori* be so. Because of the breadth of the

distribution of activity values prior to a large event, we suspect some other feature will be necessary in order to make predictions with alarm times which are significantly less. Thus it may ultimately be that the heterogeneity of the earth will lead to phenomena which probe a wider degree of time scales than those which are available in the UBK model, and ultimately then also to more precise predictions.

*Algorithm Optimization:*

In the UBK model, optimization of the  $Q$  function for activity with respect to space and time windows leads to selection of lengths which scale with  $\xi$  and time windows of order  $1/3$  the mean recurrence interval, which are the length and time scales over which correlations have been previously observed to grow prior to a large event [Carlson and Langer, 1989b; Shaw et al., 1991]. It is a positive feature that the algorithms recognize these relevant length and time scales, however, it leaves open the question of what will happen when the algorithms are applied to fault models for which there is no break in the scaling behavior. In such models (see, e.g. Chen, et al. [1991]) typically the dynamics have no inherent length or time scale so the behavior of  $Q$  as a function of box size may be very different.

The optimization issue perhaps most relevant to applications of the pattern recognition algorithms to the earth, is that of stability of prediction for independent data (catalogs not used during the learning procedure). In the model, we find that for activity alone, catalogs containing one large event cycle are sufficient for stability. If in the earth correlations in seismicity based precursors also do not extend in time beyond a single cycle, then our results suggest that substantial improvements in predictability may be expected as data bases increase to times of order the mean repeat time for large events.

*Acknowledgements:* In the course of this work we have profited greatly from discussions with V. Keilis-Borok, A. Gabrielov, D. Turcotte, J. Dieterich, G. Swindle, and especially J. S. Langer. The work of JMC was supported by a grant from the Alfred P. Sloan Foundation and NSF grant DMR-9212396. The work of SLP was supported by an INCOR grant from the CNLS at Los Alamos National Laboratories. The work of BES was supported by the SCEC grant USC-572726, and USGS grant 1434-93-G-2284. The work of JMC and BES was also supported by the National Science Foundation under Grant PHY89-04035.

#### REFERENCES

- Aki, K.J., Magnitude-frequency relation for small earthquakes; a clue to the origin of  $f_{max}$  of large earthquakes, *J. Geophys. Res.*, *92*, 1349-1355 (1987).
- Archuletta, R.J., E. Cranswick, C. Mueller, and P. Spudich, Source parameters of the 1980 Mammoth Lakes, California earthquake sequence, *J. Geophys. Res.*, *87*, 4595-4607, 1982.
- Bak, P., C. Tang, and K. Wiesenfeld, Self-organized criticality: an explanation of  $1/f$  noise, *Phys. Rev. Lett.*, *59*, 381-384, 1987.
- Bakun, W.H., C.G. Buffe, and R.M. Stewart, Body wave spectra of central California earthquakes, *Bull. Seismol. Soc. Am.*, *66*, 363-84, 1976,
- Burridge, R., and L. Knopoff, Model and theoretical seismicity, *Bull. Seismol. Soc. Am.*, *57*, 3411-3471, 1967.
- Carlson, J.M., Time intervals between characteristic earthquakes and correlations with smaller events: an analysis based on a mechanical model of a fault, *J. Geophys. Res.*, *96*, 4255-4267, 1991.
- Carlson, J.M., J.S. Langer, B.E. Shaw, and C. Tang, Intrinsic properties of a Burridge-Knopoff model of an earthquake fault, *Phys. Rev. A*, *44*, 884-897, 1991.

- Carlson, J.M. and J.S. Langer, Properties of earthquakes generated by fault dynamics, *Phys. Rev. Lett.*, *62*, 2632-2635, 1989a.
- Carlson, J.M. and J.S. Langer, Mechanical model of an earthquake fault, *Phys. Rev. A*, *40*, 6470, 1989b.
- Chen, K., P. Bak, and S. Obukov, Self-organized criticality in a crack-propagation model of earthquakes, *Phys. Rev. A* *43*, 625-630, 1991.
- Davis, P.M., D.D. Jackson, and Y.Y. Kagan, The longer it has been since the last earthquake, the longer the expected time till the next?, *Bull. Seismol. Soc. Am.*, *79*, 1439-1456, 1989.
- Davison, F.C., Jr., and C.H. Scholz, Frequency-moment distribution of earthquakes in the Aleutian Arc: a test of the characteristic earthquake model, *Bull. Seismol. Soc. Am.*, *75*, 1349-1362, 1985.
- Dieterich, J.H. An alternate null hypothesis, *U.S. Geol. Sur. Open File Rep. 88-398*, 1992.
- Gabrielov, A.M., T.A. Levshina, and I.M. Rotwain, Block model of earthquake sequence, *Phys. Earth Planet. Inter.*, *61*, 18-28, 1990.
- Healy, J.H., V.G. Kossobokov, and J.W. Dewey, A test to evaluate the earthquake prediction algorithm M8, *U. S. Geo. Sur. Open File Rep. 92-401*, 1992.
- Kanamori, H., The nature of seismicity patterns before large earthquakes, in *Earthquake Prediction, an International Review*, Maurice Ewing Series, Vol. 4, ed. D.W. Simpson and P.G. Richards, Amer. Geo. Un., Washington, D.C., 1-19, 1981.
- Keilis-Borok, V.I., and I.M. Rotwain, Diagnosis of time of increased probability of strong earthquakes in different regions of the world: algorithm CN, *Phys. Earth Planet. Inter.*, *61*, 57-72, 1990a.
- Keilis-Borok, V.I., and V.G. Kossobokov, Premonitory activation of earthquake flow: algorithm M8, *Phys. Earth Planet. Inter.*, *61*, 73-83, 1990b.
- Keilis-Borok, V.I., L. Knopoff, V.G. Kossobokov, and I. Rotwain, Intermediate-term prediction in advance of the Loma Prieta earthquake, *Geophys. Res. Lett.*, *17*, 1461-1464, 1990c.
- Kiremidjian, A.S. and T. Anagnos, Stochastic slip-predictable model for earthquake occurrences, *Bull. Seismol. Soc. Am.*, *74*, 739-755, 1984.
- Langer, J.S. and C. Tang, Rupture propagation in a model of an earthquake fault, *Phys. Rev. Lett.*, *67*, 1043-1046, 1991.
- Langer, J.S., Models of crack propagation, *Phys. Rev. A* *46*, 3123 (1992).
- Malin, P.E., S.N. Blakeslee, M.G. Alvarez, and A.J. Martin, Microearthquake imaging of the Parkfield asperity, *Science*, *244*, 557, 1989.
- McNalley, K.C., and J.B. Minster, Nonuniform seismic slip rates along the Middle American Trench, *J. Geophys. Res.*, *86*, 4949-4959 1981.
- Mogi, K., Study of elastic shocks caused by the fracture of heterogeneous material and its relation to earthquake phenomena, *Bull. Earthq. Res. Inst., Univ. Tokyo*, *40*, 125-173, 1962.
- Molchan, G.M., and Kagan, Y.Y., Earthquake prediction and its optimization, *J. Geophys. Res.*, *97*, 4823-4838, 1992.

- Molchan, G.M., Structure of optimal strategies in earthquake prediction, *Tectonophysics*, 193, 267-276, 1991.
- Nishenko, S.P., and R. Buland, A generic recurrence interval distribution for earthquake forecasting, *Bull. Seismol. Soc. Am.*, 77, 1382-1399, 1987.
- Pacheco, J.F., C.H. Scholz, and L.R. Sykes, Changes in frequency-size relationship from small to large earthquakes, *Nature*, 235, 71-73, 1992.
- Scholz, C.H., Earthquake prediction and seismic hazard, *Earthq. Predict. Res.*, 3, 11-23, 1985.
- Schwartz, D.P. and K.J. Coppersmith, Fault behavior and characteristic earthquakes: examples from the Wasatch and San Andreas fault zones, *J. Geophys. Res.*, 89, 5681-5698, 1984.
- Shaw, B.E., J.M. Carlson, and J.S. Langer, Patterns of seismic activity preceding large earthquakes, *J. Geophys. Res.*, 97, 479, 1992.
- Shaw, B.E., Moment spectra in a simple model of an earthquake fault, *Geophys. Res. Lett.*, to appear, 1993 a.
- Shaw, B.E., Generalized Omori Law for aftershocks and foreshocks from a simple dynamics, *Geophys. Res. Lett.*, to appear, 1993 b.
- Shimazaki, K. and T. Nakata, Time predictable recurrence model for large earthquakes, *Geophys. Res. Lett.*, 7, 279-282, 1980.
- Sykes, L.R. and M. Tuttle, A seismic precursor to the Loma Prieta earthquake, rupture zones of historic nearby earthquakes and seismic potential of the Hayward fault, *USGS Monograph*, March 25, 1991.
- Thatcher, W., The earthquake deformation cycle, recurrence, and the time- predictable model, *J. Geophys. Res.*, 89, 5674-5680, 1984.
- Vasconcelos, G.L., M.S. Vieira, and S.R. Nagel, Phase transitions in a spring- block model of earthquakes, *Physica A*, 191, 69-74, 1992.
- Ward, S.N., An application of synthetic seismicity in earthquake statistics - the Middle America Trench, *J. Geophys. Res.*, 97, 6675-6682, 1992.
- Wesnousky, S., C.H. Scholz, K. Shimazaki, and T. Matsuda, Earthquake frequency distribution and the mechanics of faulting, *J. Geophys. Res.*, 88, 9331-9340, 1983.
- Working Group on California Earthquake Prediction, Probabilities of large earthquakes occurring in California on the San Andreas fault, *U.S. Geol. Sur. Open File Rep. 88-398*, 1988.
- Working Group on California Earthquake Prediction, Probabilities of large earthquakes in the San Francisco Bay Region, California, *U.S. Geological Survey Circular*, 1053, 1990.
- Wyss, M., Precursors to large earthquakes, *Earthq. Predict. Res.*, 3, 519-543, 1985.

## FIGURES

(1). A sample catalog illustrating the events which take place as a function of space and time in the UBK model. Time on the vertical axis is measured relative to the inverse loading speed, so that values on that axis represent  $t\nu = \delta U$ , i.e. the net displacement of initially adjacent points on opposite sides of the fault. A line segment is drawn through all of the blocks which slip during an event, and a cross marks the position of the epicenter of each large event. Individual events are also quite complex, with spatially irregular slip which unfortunately cannot be illustrated simultaneously on a plot such as this. Figure (a) represents only a fraction (both in space and time) of the full catalog which is considered, and (b) is an expansion of the precursory activity for one the large events in (a). Unless explicitly stated otherwise, the numerical results illustrated in the figures that follow will be for a system of size  $N = 8192$ , with  $\ell = 10$ ,  $\sigma = .01$  and  $\alpha = 3$ . The full catalog (excluding one block events— the exclusion of these was not seen to alter the results) consists of 114,000 events, 1848 of which are large events and corresponds to a total displacement of  $\delta U = 122$ .

(2). Log Frequency  $\ln[D(\mu)]$  vs. magnitude  $\mu$  for the UBK model. Here  $D(\mu)d\mu$  is the number of events per unit length per unit time (time is measured in units of the inverse loading speed, as in Fig. 1) in the magnitude range  $[\mu, \mu + d\mu]$ . The small events satisfy the Gutenberg–Richter law  $D(\mu) = Ae^{-b\mu}$  with  $b = 1$ , while the large events occur at a rate which is in excess of the extrapolated rate of small events. The crossover between small and large events is denoted by  $\tilde{\mu} = \ln\tilde{M}$ , where  $\tilde{M} \approx 2/\alpha$ . The peak in the large events distribution corresponds roughly to a rupture length  $\xi^* \approx 10\tilde{\xi}$  which is well below the system size. The magnitude  $\mu^*$  typically associated with such events is indicated in the figure. In the corresponding integrated distribution (i.e. where the frequency of events with magnitude in the range  $[\mu, \infty)$  is plotted) the peak is replaced by a flat shoulder. We choose to plot the differential distribution because the location of the crossover magnitude  $\tilde{\mu}$  is suppressed in the integrated distribution.

(3). Cumulative slip as a function of time for a representative patch along the fault. While the small events overall are much more frequent than the large events, all of the visible displacement is associated with large events. The lines illustrate the best least-squares fits to the upper and lower corners of the staircase, and thus represent the best fits to the slip-predictable and time-predictable models, respectively. Clearly, the sequence of events is not periodic, and although neither the slip-predictable model nor the time-predictable model work particularly well, a more complete test (see Fig. 4) indicates that the time-predictable model does somewhat better (in particular, the root mean square deviation from the linear fit is less for the time-predictable model).

(4). Tests for correlations between seismic moments and time intervals for subsequent large events. Here  $T_i$  and  $T_{i+1}$  are the time intervals preceding large subsequent events of moment  $M_i$  and  $M_{i+1}$ , respectively. Pairs of events in which the epicenters lie within  $\tilde{\xi}$  of one another are considered. Fig. (a) illustrates a test of the time-predictable model which, if correct, would lead to collapse of the data for  $T_{i+1}$  vs.  $M_i$  onto a line. Fig. (b) illustrates a test of the slip-predictable model which, if correct, would lead to a collapse of the data for  $M_i$  vs.  $T_i$  onto a line. In (c) and (d) we test for correlations between  $M_i$  and  $M_{i+1}$  as well as  $T_i$  and  $T_{i+1}$ , respectively. While none of the graphs show significant correlations, compared to the others (a) minimizes the least squares deviation to the best linear fit, which is shown in that case. However, our primary conclusion from this data is that while short catalogs may sometimes suggest some correlation such as those tested here, none of these simple prediction schemes is reliable even for the simple UBK model.

(5). Local recurrence intervals for large events on the UBK model, scaled by the mean recurrence interval  $\bar{T} = .558/\nu$ . Figure (a) illustrates the density (i.e. the probability of a repeat time in the interval  $[T/\bar{T}, T/\bar{T} + dT/\bar{T}]$ ) while (b) represents the cumulative distribution along with the best fits to Gaussian (G), Weibull (W), and lognormal (L) distributions (shifted for convenience). Comparison of the root mean square deviation for

each of the fits indicates that the Gaussian (starting at  $T/\bar{T} = 0$ , i.e. omitting unphysical negative intervals) provides the best fit, followed closely by the Weibull, and finally by the lognormal.

(6). Success curve for time interval prediction. Here we plot the fraction of large events predicted ( $p_1$ ) vs. the fraction of time occupied by alarms ( $p_2$ ). The octagons correspond to local predictions, while the dashed line corresponds to predictions made in spatially coarse grained windows of size  $3\tilde{\xi}$  (we show the second curve for comparison to the results obtained for the intermediate term algorithms). The upper curve represents a limit for prediction based upon recurrence intervals for the model. In this case, predicting 80% of the large events requires that alarms be declared roughly 35% of the time. Each point on the curve corresponds to a different value of the threshold time  $t_0$  at which an alarm will be issued relative to the time of the last large event. This curve can be deduced directly from the time interval distribution illustrated in Fig. 5a, where, for example, the fraction of events successfully predicted corresponds to the relative weight of intervals greater than  $t_0/\bar{T}$  in the density.

(7). Quality function  $Q$  for time interval prediction. Here we plot  $Q = p_1 - p_2$  ( $p_3 = 0$  since there are no false alarms with this method) as a function of  $p_2$  for the data illustrated in Fig. 6. As previously octagons represent local forecasts, and the dashed line represents the coarse grained results.

(8). Distribution of values of the activity precursor  $f_1(\Delta s, \Delta t)$  evaluated in space-time windows  $\Delta s = 3\tilde{\xi}$  and  $\Delta t/\bar{T} = .36$ . Both the full time average  $P(f_1)$  as well as the distribution of values just prior to a large event  $P(f_1 | \text{large event})$  are illustrated. The relatively small overlap between the two distributions suggests that activity should be a reasonably good intermediate term predictor for the UBK model.

(9). Success curves for intermediate term precursor functions  $f_i(\Delta s = 3\tilde{\xi}, \Delta t/\bar{T} = .36)$ .

Note that for purely random prediction the fraction predicted  $p_1$  is equal to the fraction time occupied by alarms  $p_2$  (i.e. the straight line on the graph) indicating that all of the functions perform better than random prediction. In terms of the success curve, all of the functions perform better than prediction based on time intervals as well (i.e. at least for some range of  $p_2$  for the success curve for time interval prediction represented here by the dashed line lies below each of the curves shown). It is interesting to note the extent to which active zone size outperforms the other precursors, predicting nearly all of the large events when alarms occupy roughly 5% of the total time. While this is clearly the best indicator, active zone size, activity, and activity rate of change all perform substantially better than random prediction for all threshold values, predicting 90% of events with alarms on 5%, 14%, and 16% of the time, respectively. Fluctuations in activity performs somewhat worse than the others, achieving a probability gain of only about 2.7 over random prediction, compared to the long term prediction gain of 2.3 (when 90% of events are predicted).

(10). Quality functions  $Q$  for the intermediate term precursor functions illustrated in Fig. 9. Figure (a) represents results for the probability based function  $Q_P$  with  $Q_P = p_1 - p_2 - p_3$ , and the  $p_i$  are taken to be probabilities, while (b) represents results for the cost-benefit function  $Q_C$  with  $Q_C = p_1 - p_2 - p_3/3$ , and the  $p_i$  are taken to be rates. In either case, when  $Q < 0$ , from a cost-benefit standpoint it is better to do nothing (then  $Q = 0$ ). Active zone size, activity, and activity rate of change all perform reasonably well compared to doing nothing, with their  $Q$  values rising above zero by the time alarms occupy 5% of the total observation period. In comparison, fluctuations in activity almost always has  $Q < 0$ , indicating that it is a rather poor measure. Compared to the relative results for the success curve (Figs. 6 and 9) in which all of the intermediate term precursors outperformed the long term technique, here values of  $Q$  are more comparable to (and sometimes worse than) those obtained for time interval prediction (Fig. 7) because of the penalty for false alarms which is significant for all of the intermediate term precursors but which is not relevant for



time interval prediction. Note that in some applications one might be willing to tolerate a higher percentage of false alarms, and thus choose to reduce the coefficient  $|A_3|$  of  $p_3$  in  $Q$ . In that case all of the precursors considered here would have increased values of  $Q$  and thus have  $Q > 0$  most of the time.

(11). Test for independence of activity  $f_1$  and rate of change of activity  $f_2$  precursor functions. Each point in (a) represents simultaneous values of  $f_1$  and  $f_2$  at unrestricted points in time while the values plotted in (b) are the values just prior to a large event. These plots constitute projections of the joint probability distributions for  $f_1$  and  $f_2$  analogous to those illustrated for  $f_1$  in Fig. 8. While the values are clearly correlated, the nonnegligible spread in the joint distribution prior to a large event suggests that the quality of our predictions may be enhanced through a judicious combination of the two functions as described in the text.

(12). Optimization of space and time windows for the activity precursor  $f_1$ . Here  $Q_{\max}$  is plotted as a function of  $\Delta s$  and  $\Delta t/\bar{T}$  for the probability based quality function  $Q_P$ . At each space and time window,  $Q_P$  has already been optimized with respect to the threshold value  $F_1$ . Here the maximum with respect to  $\Delta s$  and  $\Delta t$  is fairly broad indicating that the algorithm is robust with respect to variations in these parameters. In particular, variations in  $Q_{\max}$  are less than 10% for time windows from ranging from .2 to .5 of the mean recurrence interval and space windows ranging from  $2\tilde{\xi}$  to  $7\tilde{\xi}$ .

(13). Cross-sections for (a) space and (b) time window optimization. Here we illustrate the danger of an injudiciously chosen quality function  $Q$ . In each case the lower curve is simply a cross-section of the results plotted in Fig. 12 ( $|A_3| = 1$ ), while the upper curve corresponds to the results obtained when the penalty for false alarms is not included ( $|A_3| = 0$ ). In (a) the intermediate value  $|A_3| = .3$  is included to illustrate that the size of the optimal spatial window is sensitive to the choice of this coefficient. The fact that the upper curves ( $|A_3| = 0$ ) are maximized for small (essentially infinitesimal) space and

time windows leads to an ill-defined optimization problem as described in the text.

(14). The effects of restricted magnitude windows. Here we plot  $Q_{\max}$  for the activity precursor as a function of lower magnitude cutoff  $\mu_{\min}$  for the catalog (events below the cutoff are omitted in our evaluation of  $f_1$ ). The steady rise in  $Q$  up to  $\mu_{\min} \approx -7.5$  is due to the decreasing number of false alarms. The curve plateaus near where  $Q$  is optimized for a threshold value of 1 event, and thereafter is governed by the probability of observing a single event of sufficient magnitude to trigger an alarm before the large event is initiated. The steep decline occurs roughly when the integrated probability of observing an event above the cutoff per unit length per unit time is less than the probability of observing a large event. Here we show results for  $\Delta t/\bar{T} = .18$  in order to clearly illustrate the bump present for intermediate magnitudes, suggesting a possible additional precursor function associated with intermediate size events.

(15). The effects of restricted catalog length. Here we consider the convergence of the intermediate term prediction algorithm as a function of the catalog length (in time). The space and time windows for the algorithm are fixed at  $\Delta s = 3\tilde{\xi}$  and  $\Delta t/\bar{T} = .18$  (the optimal  $\Delta t$  was not chosen in order to allow for greater range in catalog length). In each case, roughly 100 catalogs were combined, and optimized with respect to the threshold  $F_1$ , so that for each catalog length  $F_1$  was set by the maximum average  $\bar{Q}_{\max}$  for the set of catalogs of that length. In (a) we plot this average value as a function of catalog length. In (b) we plot the width of the distribution of  $Q$  values (for the independent catalogs with the threshold fixed at  $F_1$ ) as a function of catalog length. Interestingly the mean converges to its optimal value and the width approaches zero once the catalog length becomes roughly of order the mean recurrence interval.

Fig. 1(a)

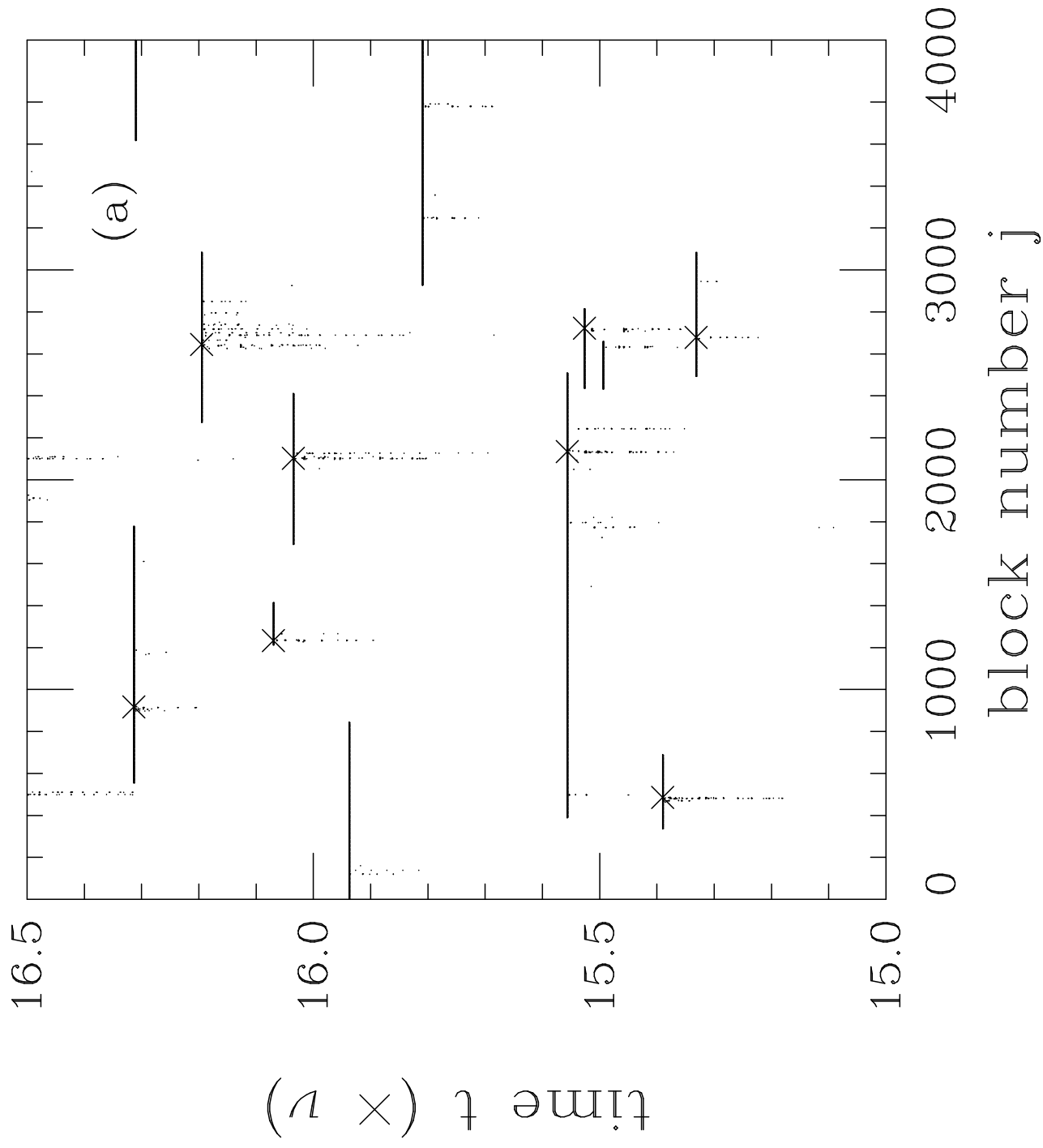




Fig. 2

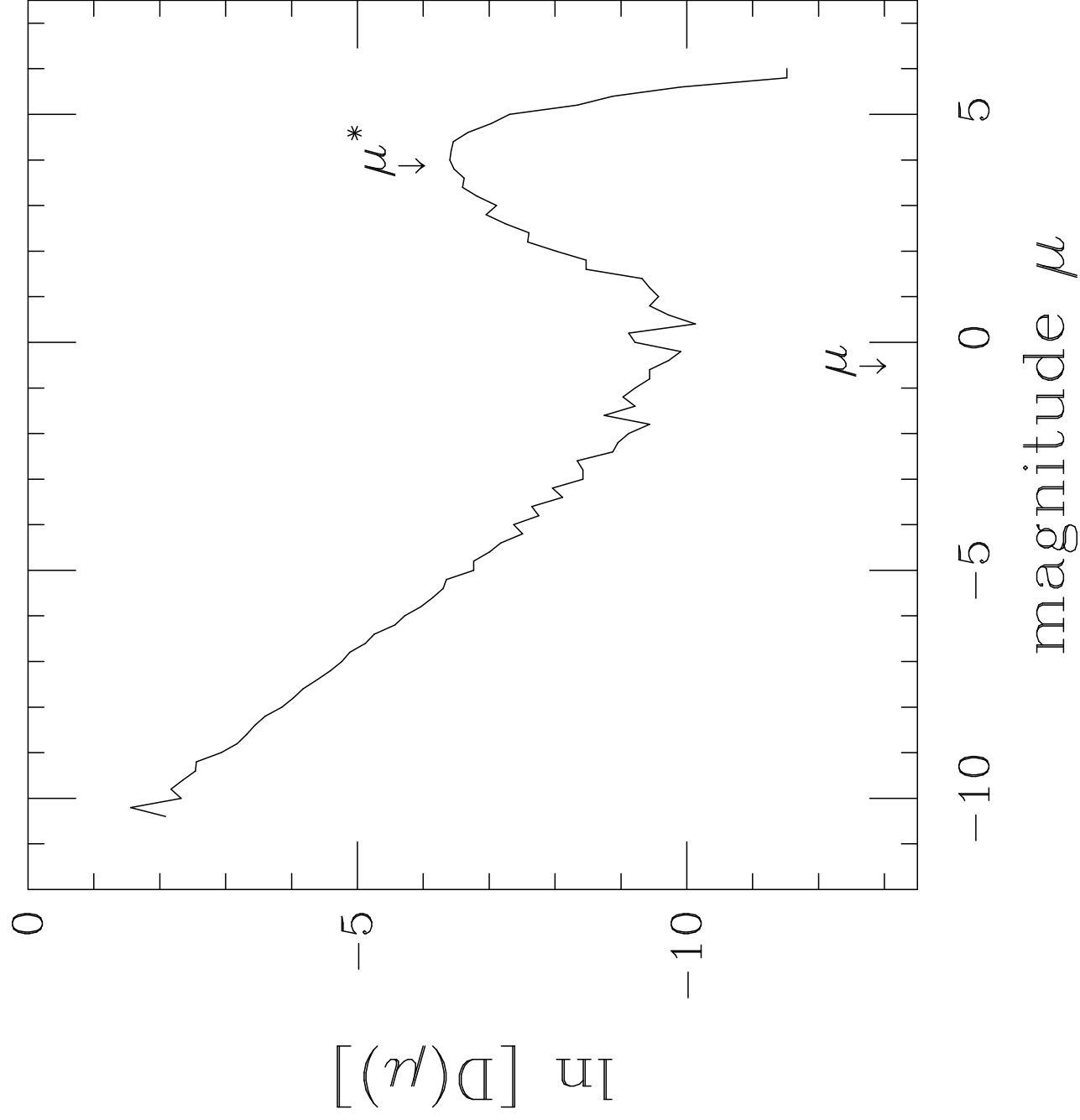


Fig. 3

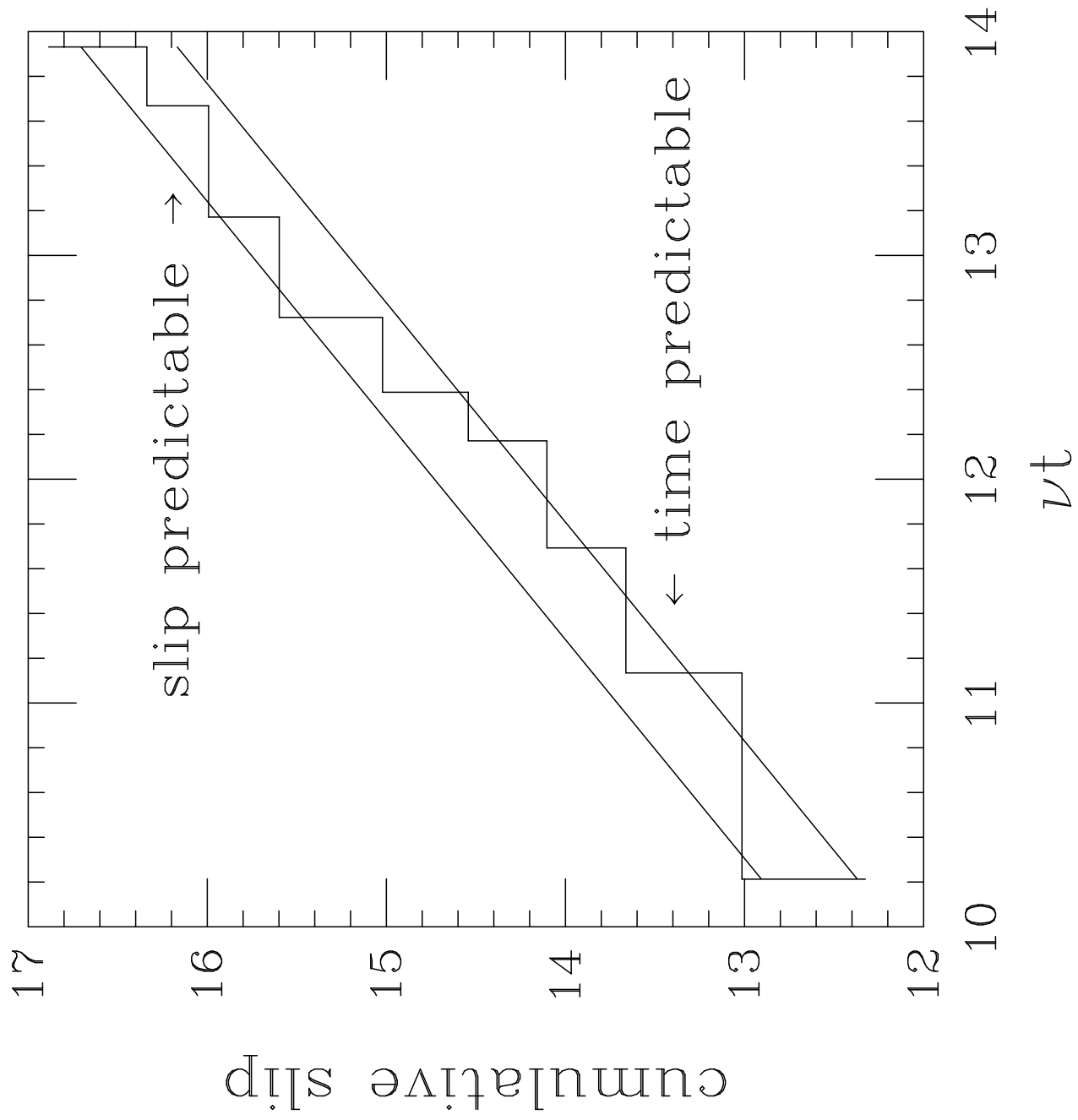


Fig. 4(a)

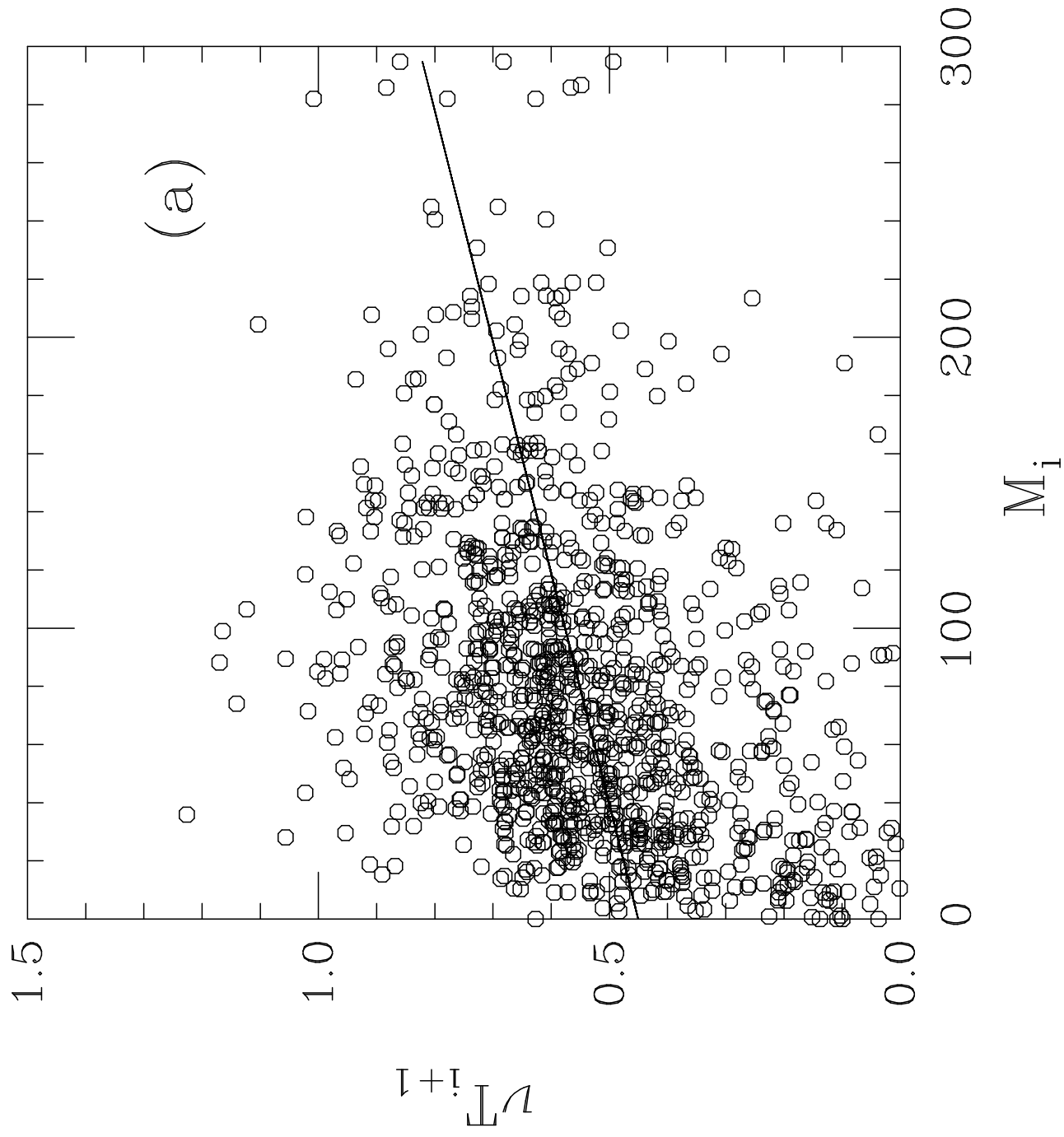


Fig. 4(b)

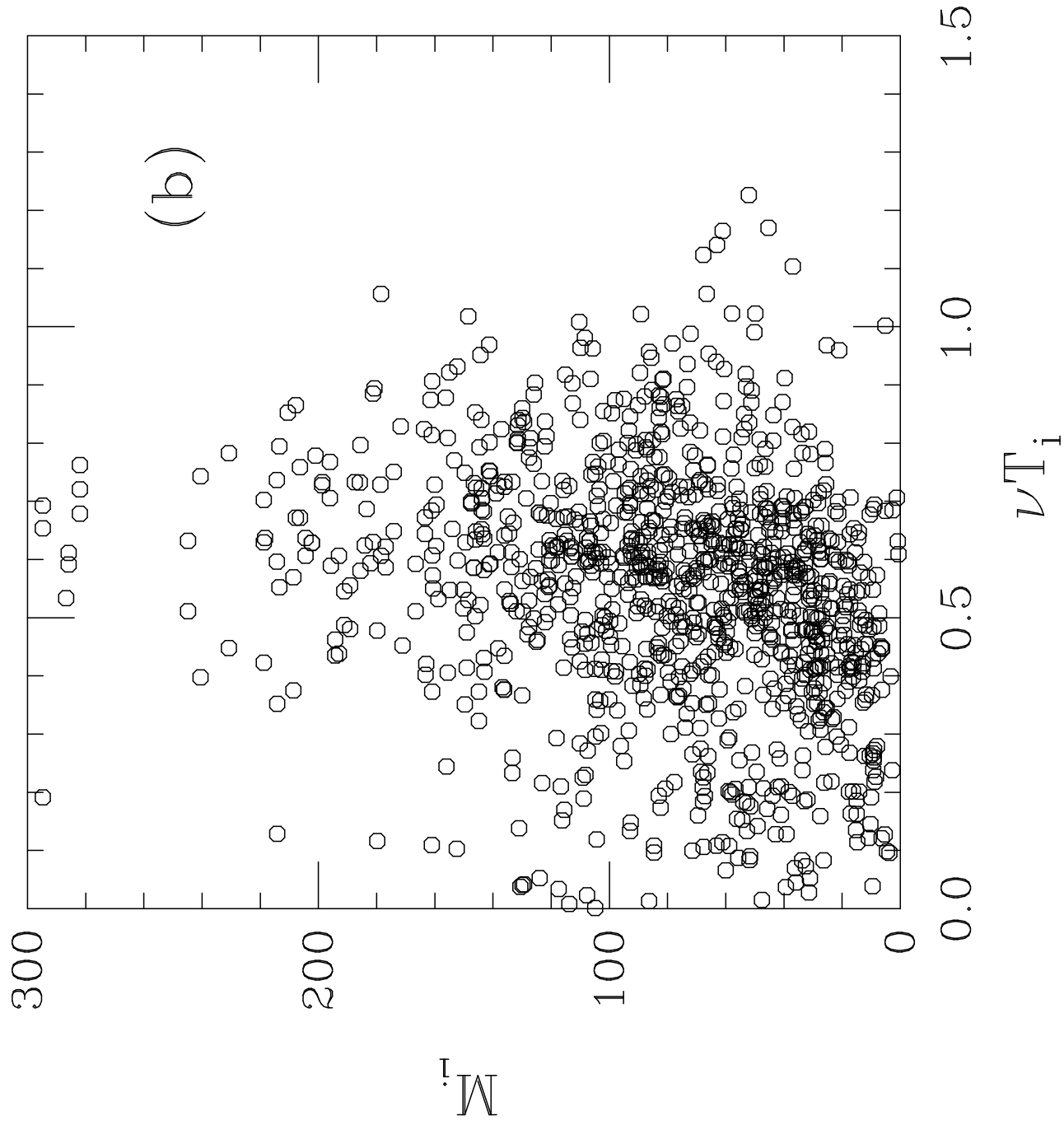




Fig. 4(c)

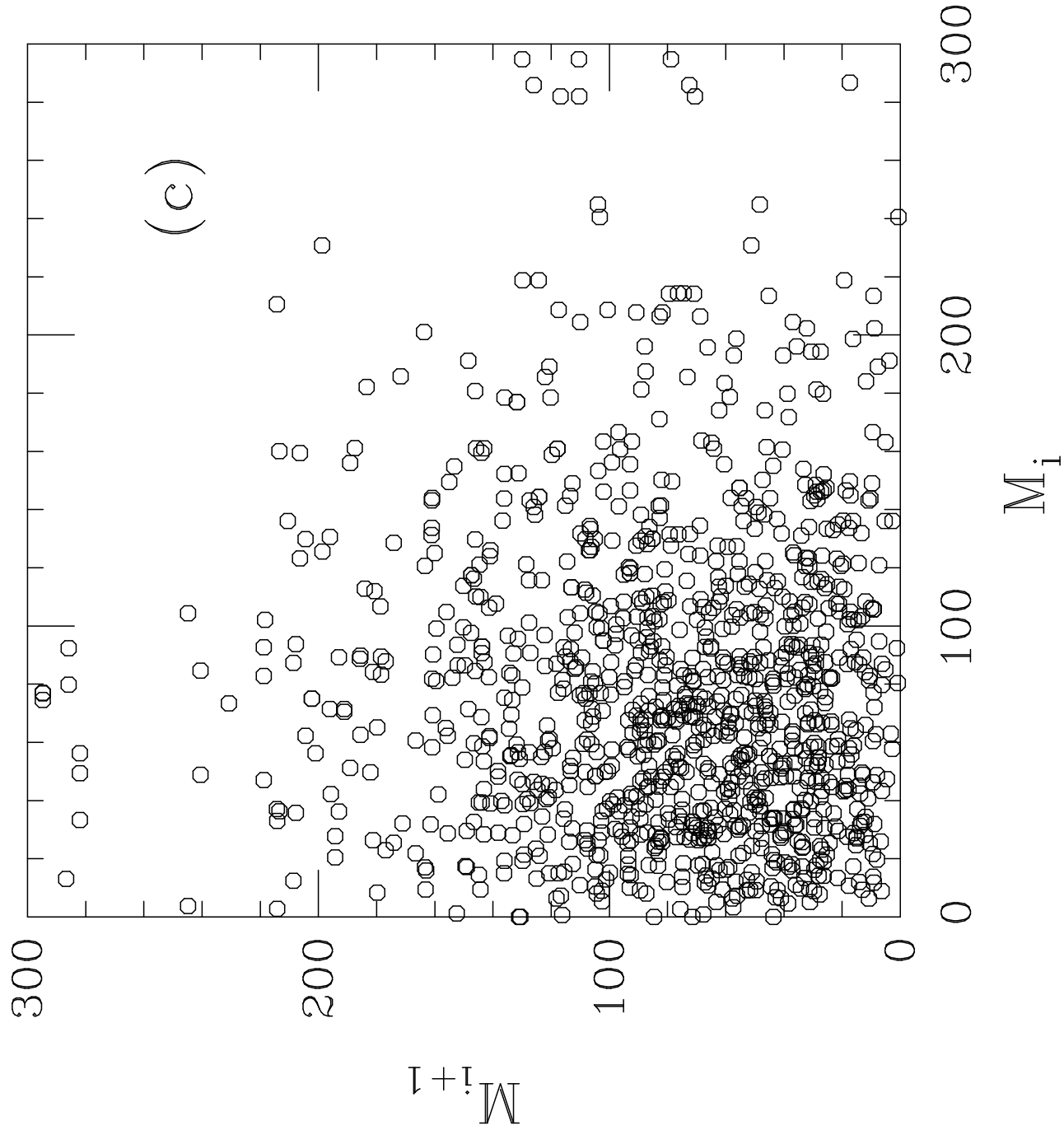


Fig. 4(d)

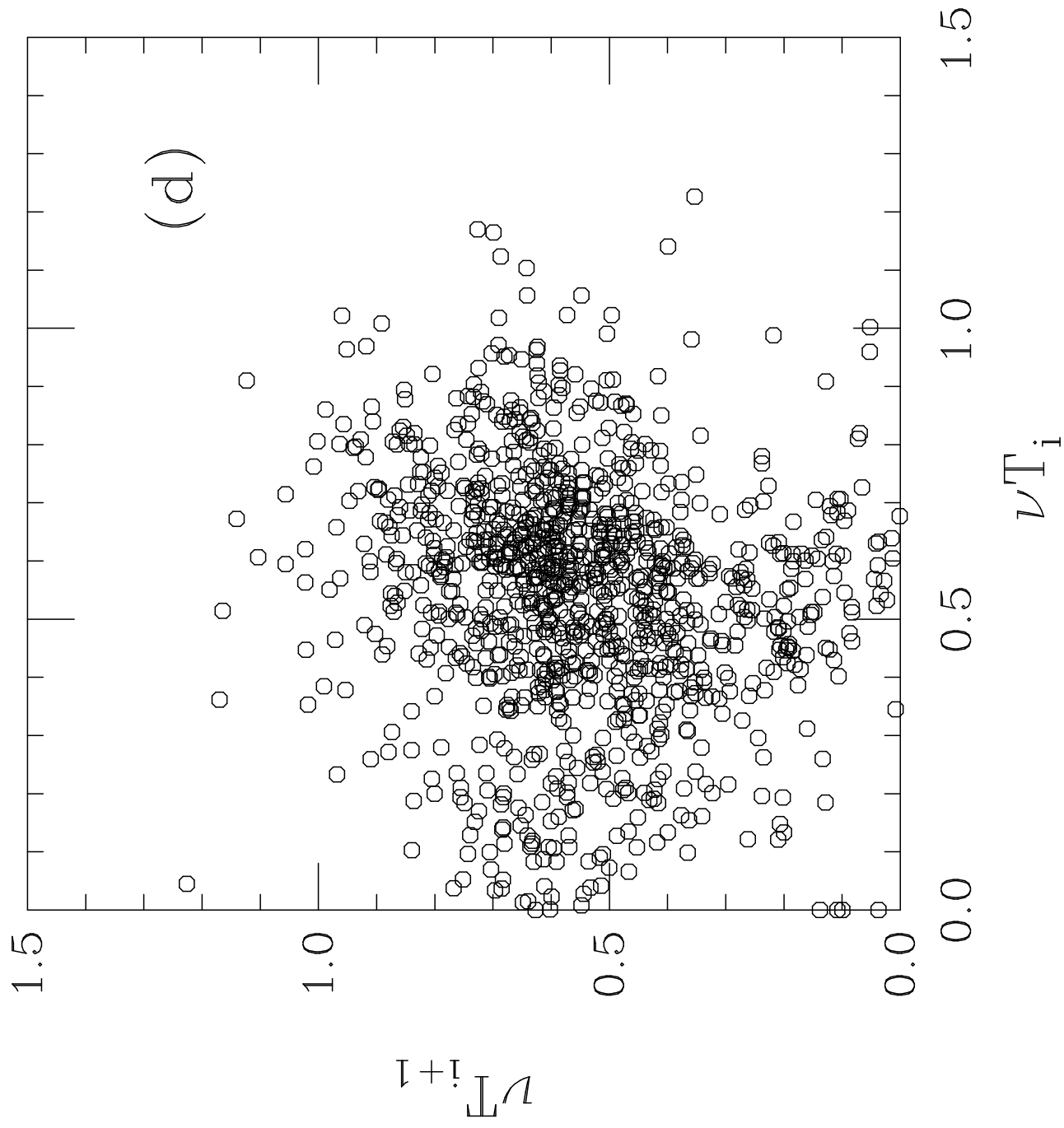


Fig. 5(a)

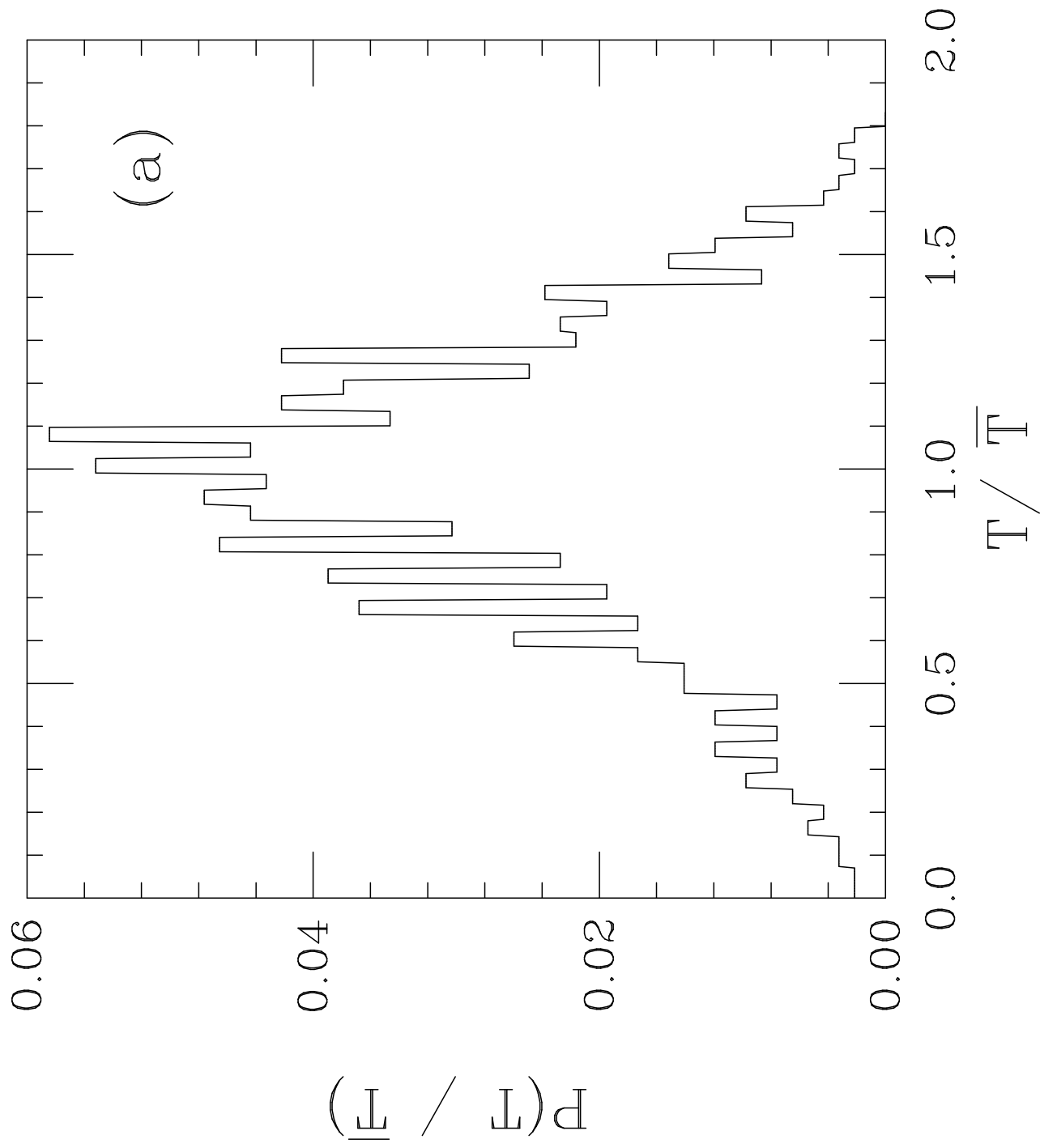


Fig. 5(b)

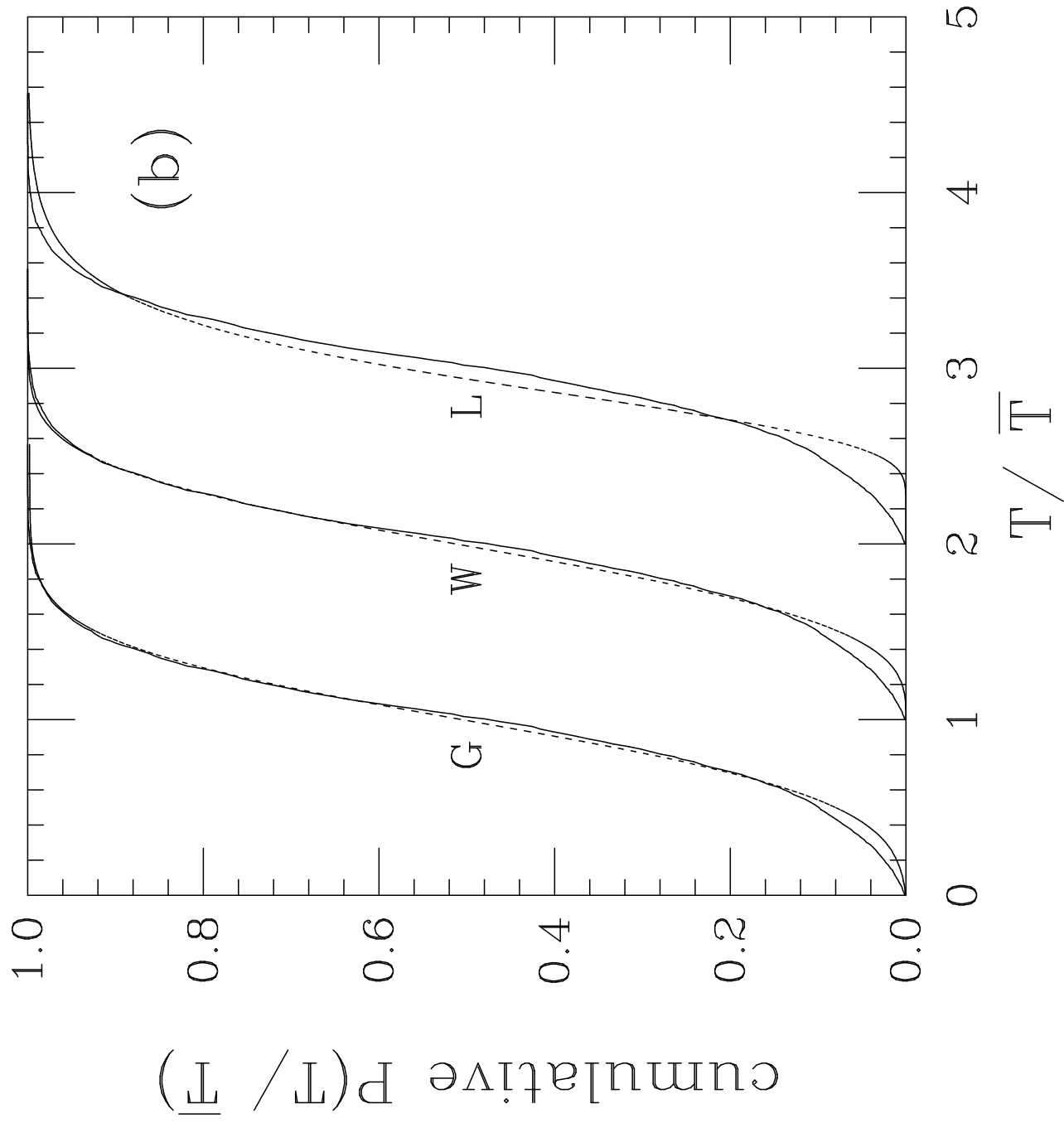


Fig. 6

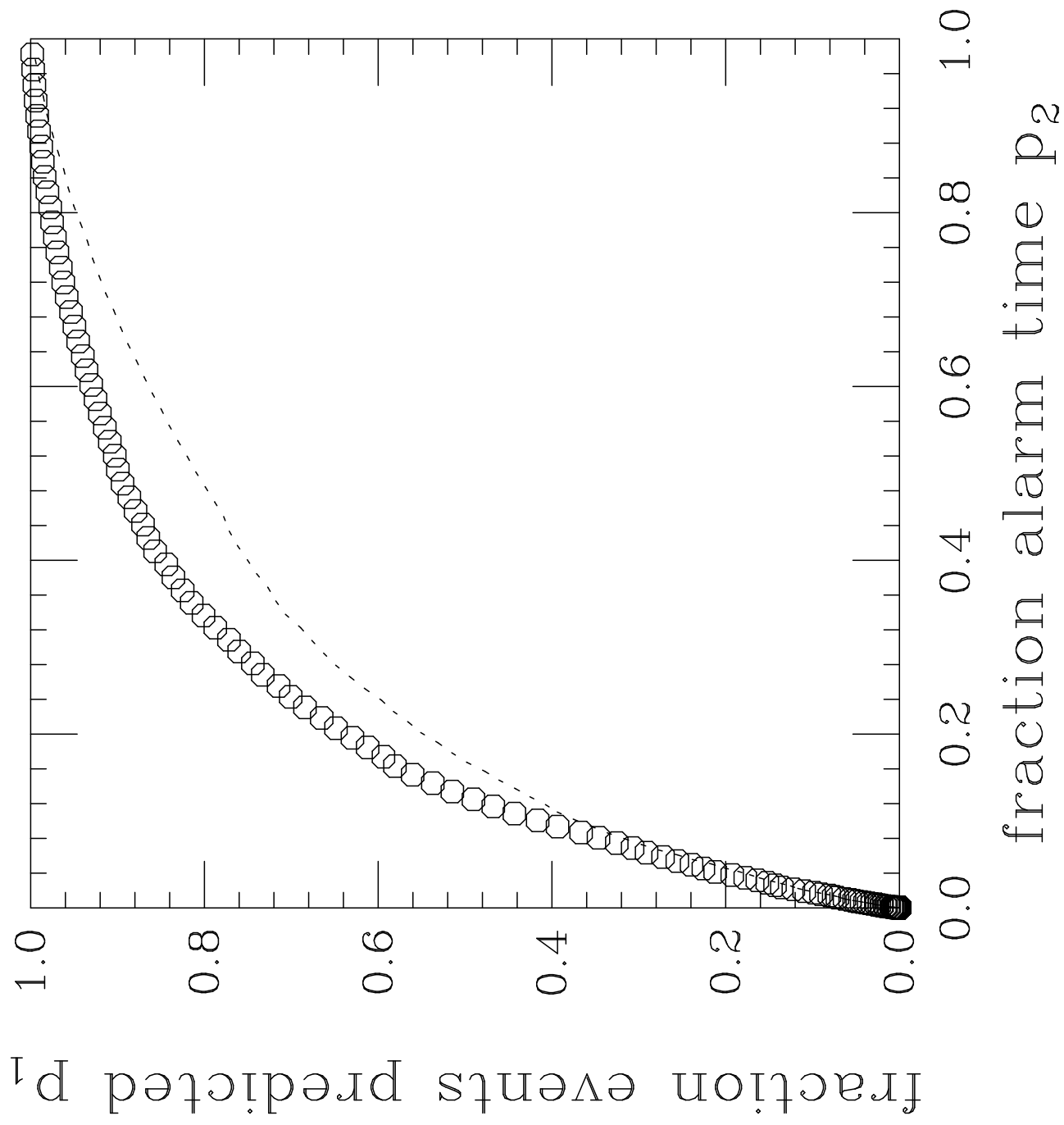


Fig. 7

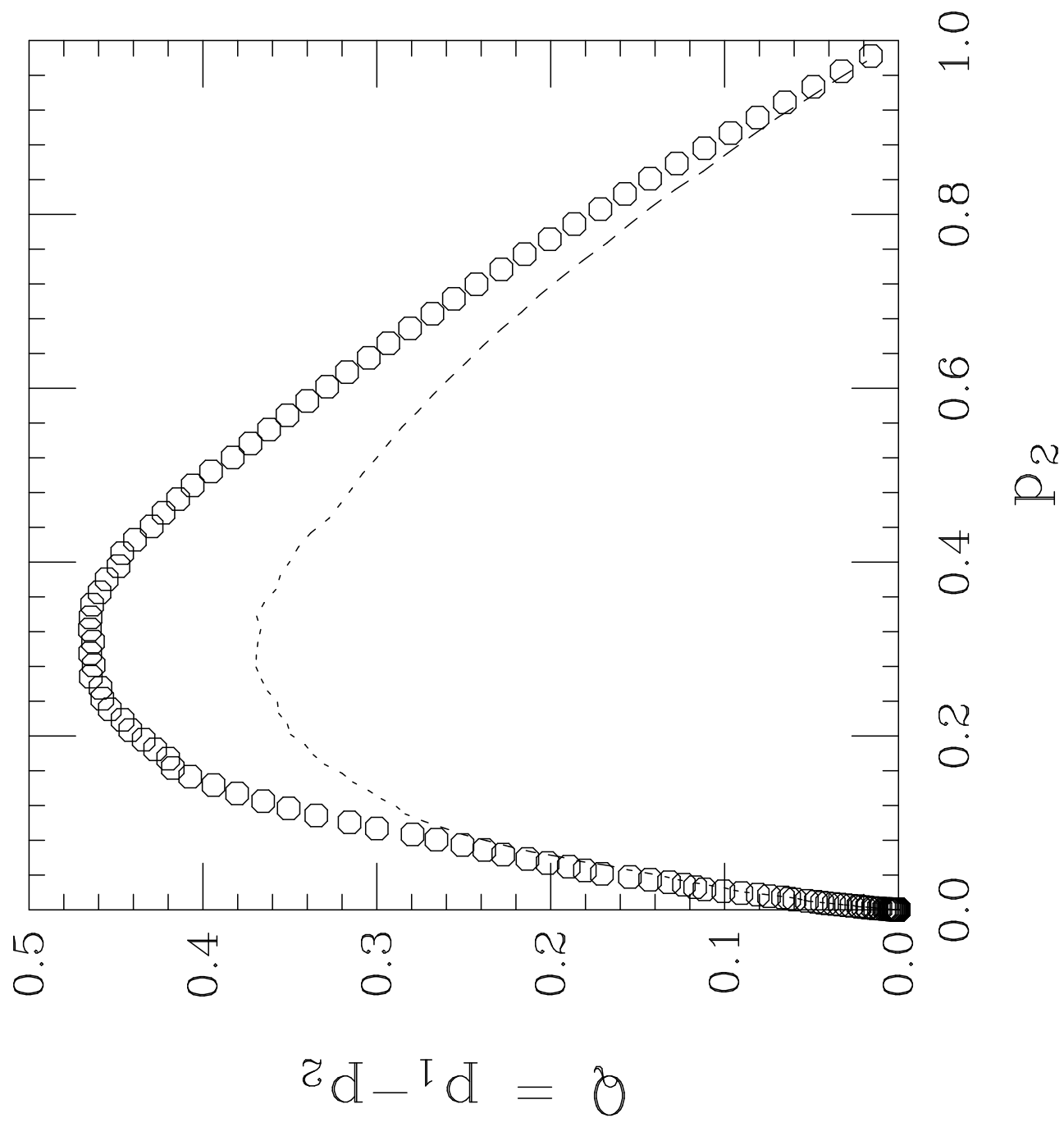


Fig. 8

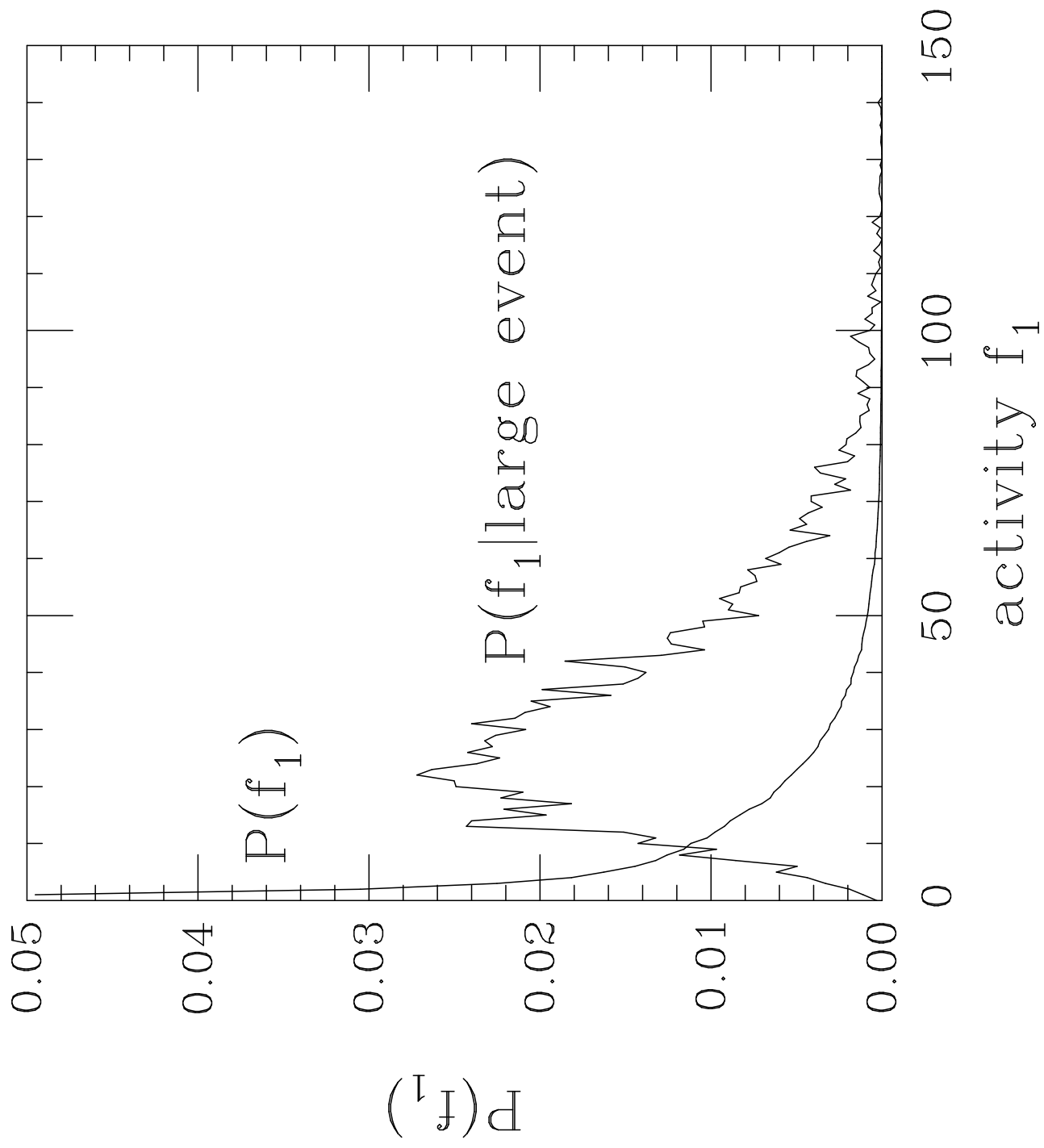


Fig. 9

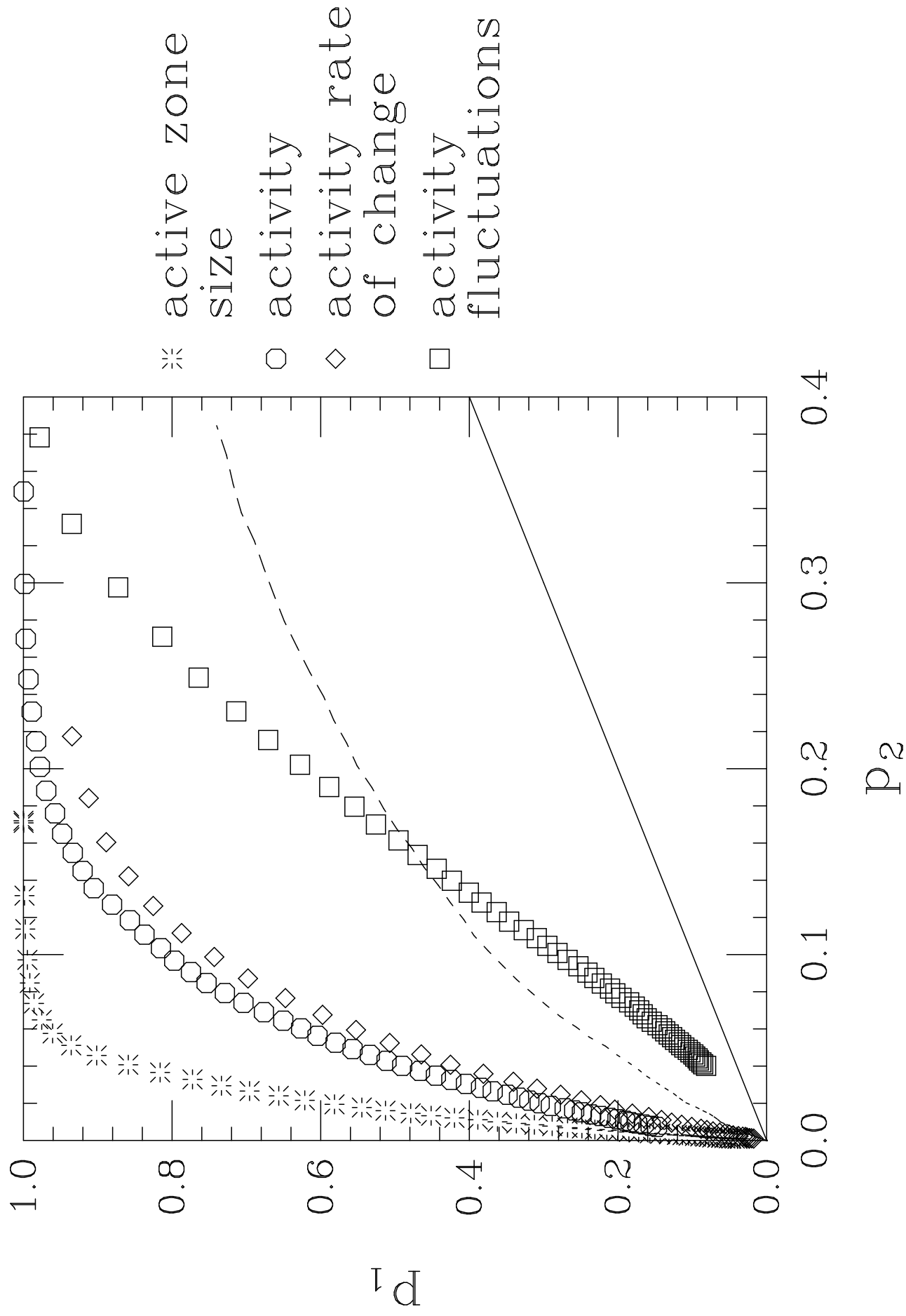




Fig. 10(a)

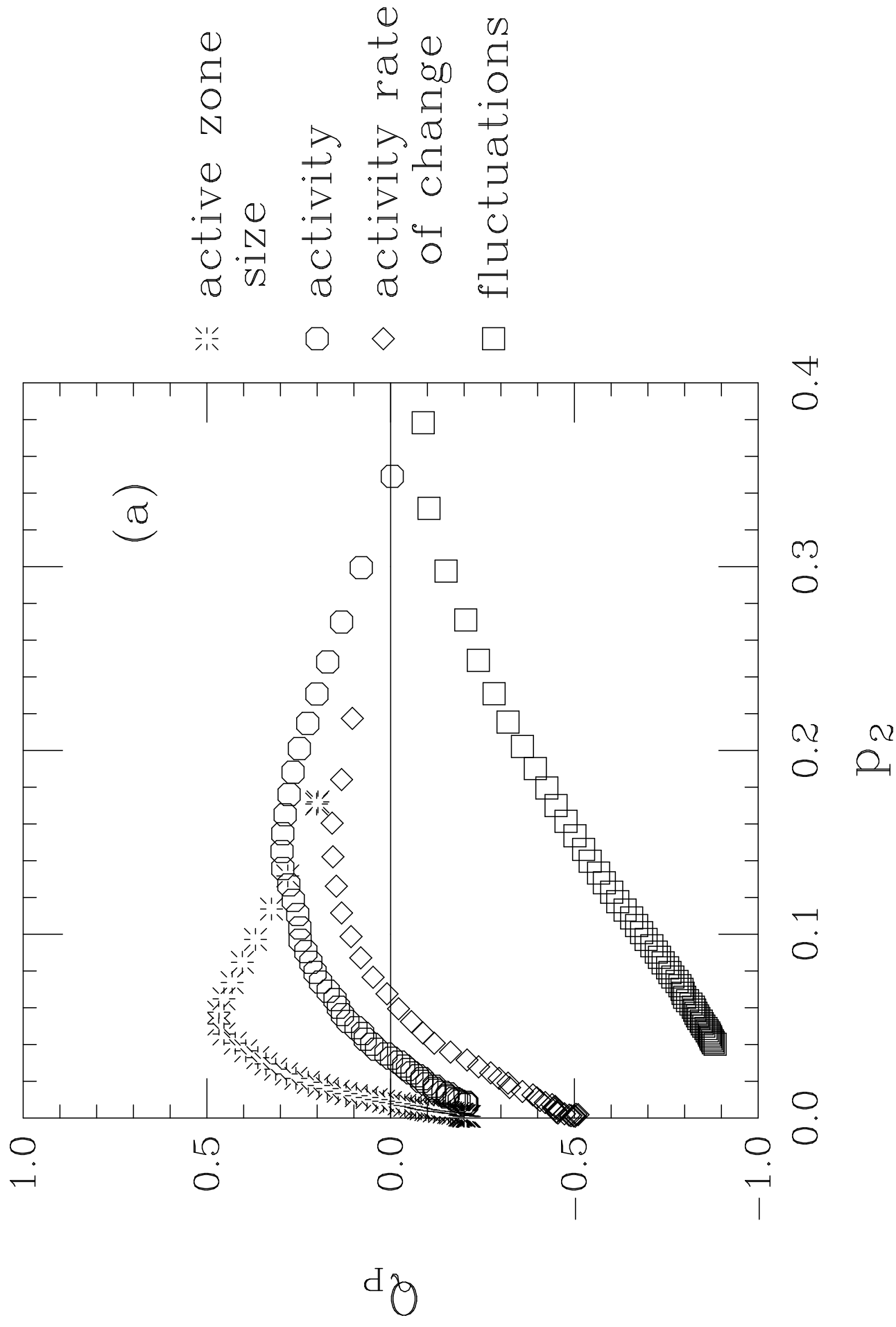


Fig. 10(b)

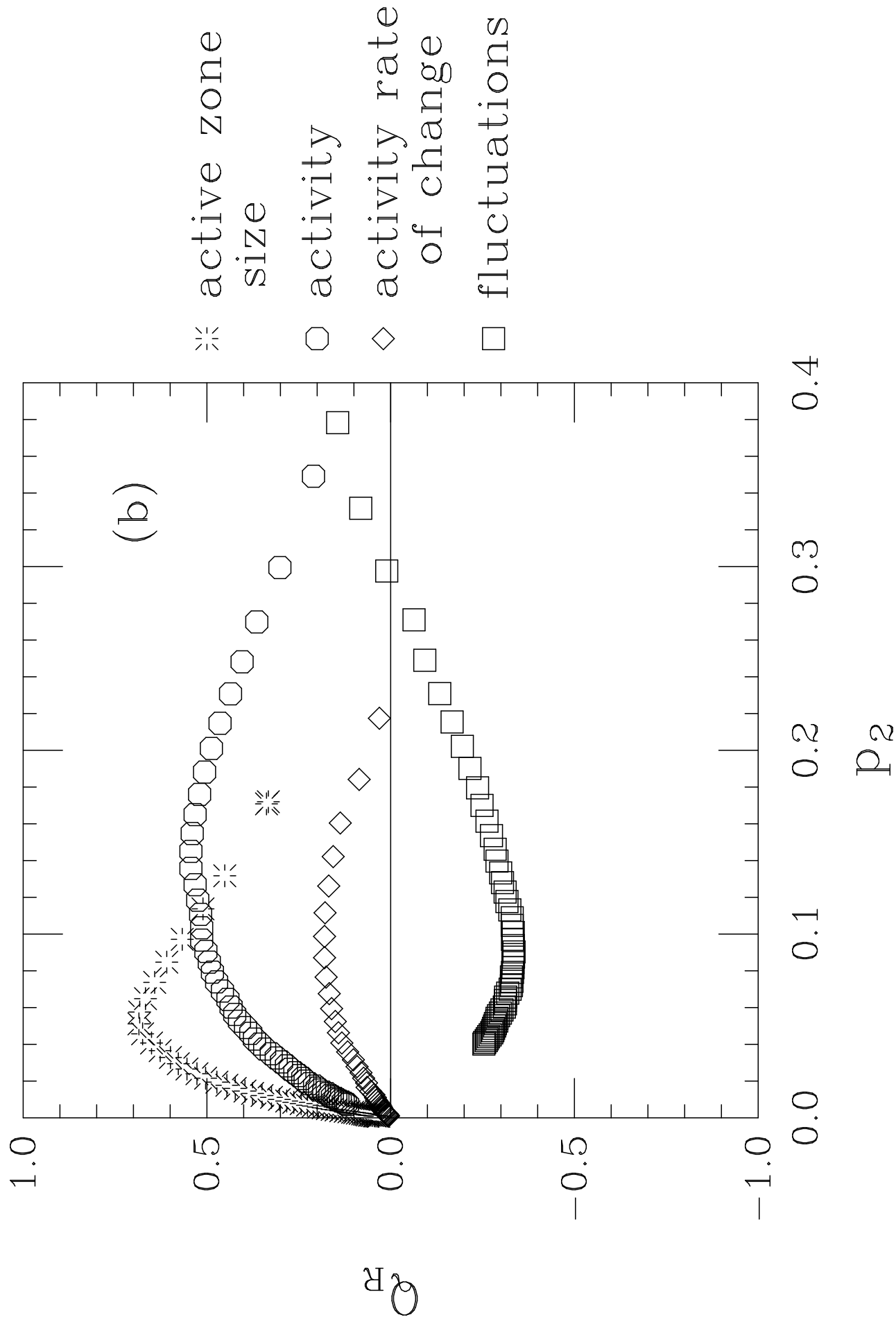


Fig. 11(a)

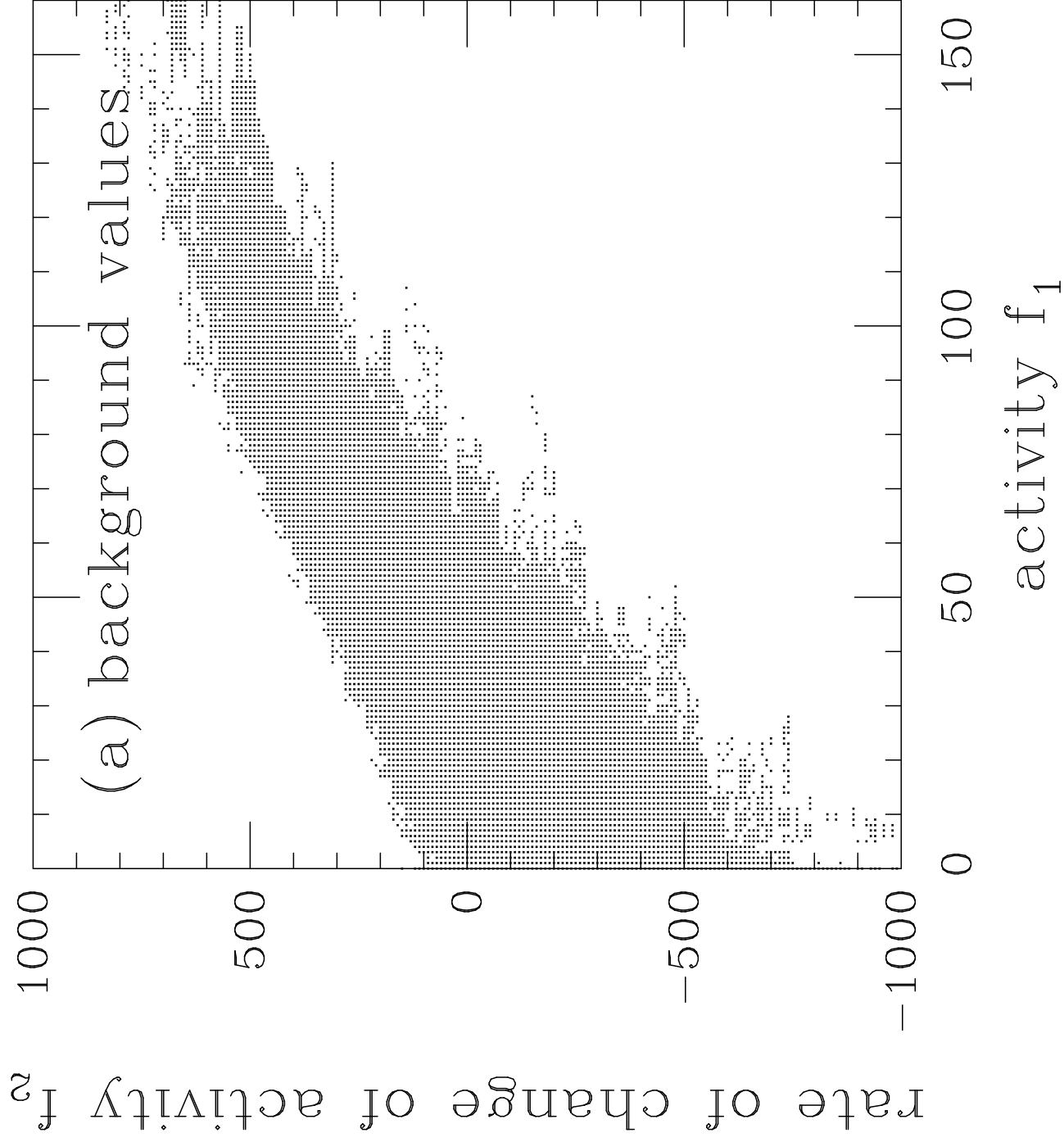
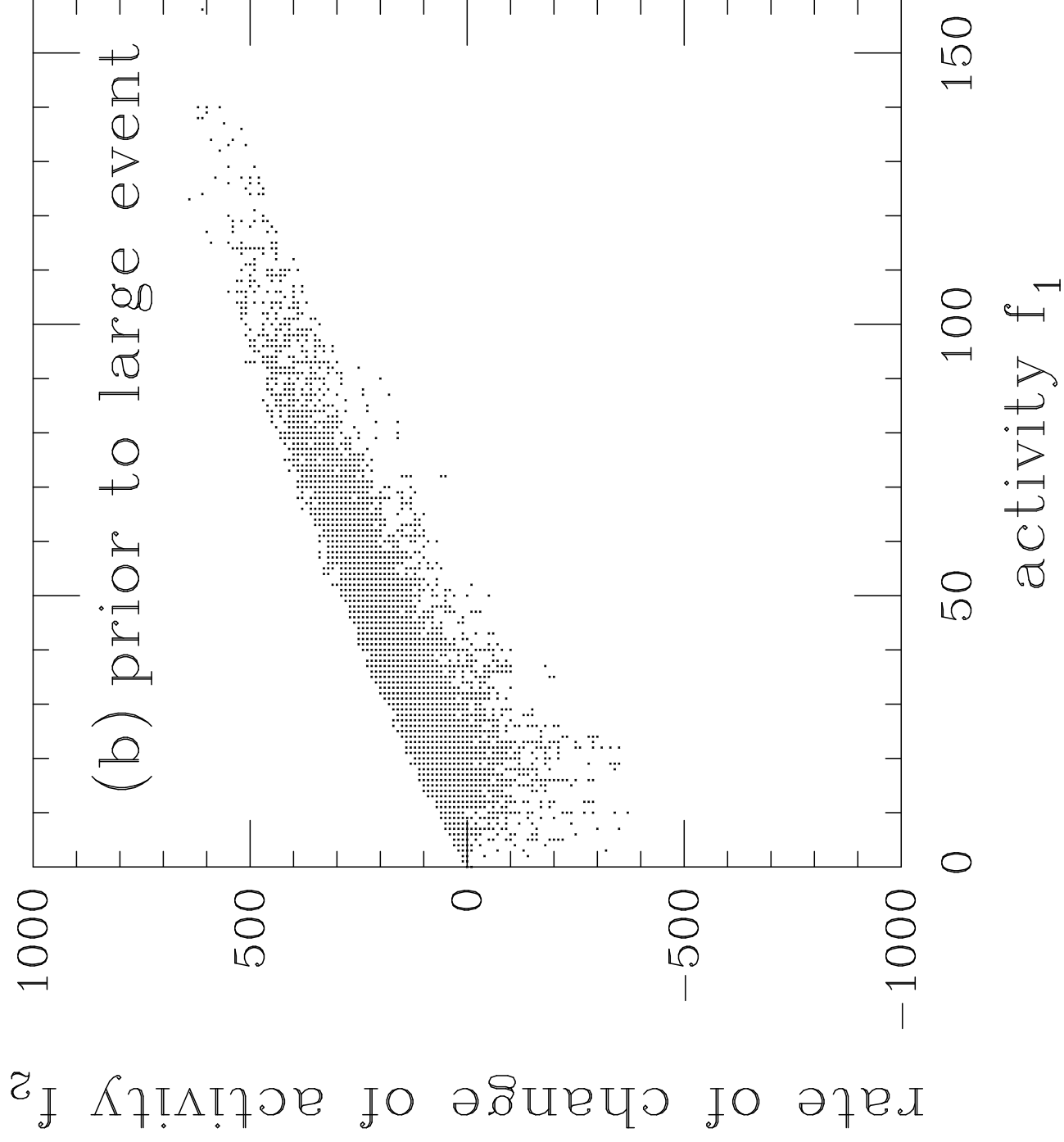


Fig. 11(b)



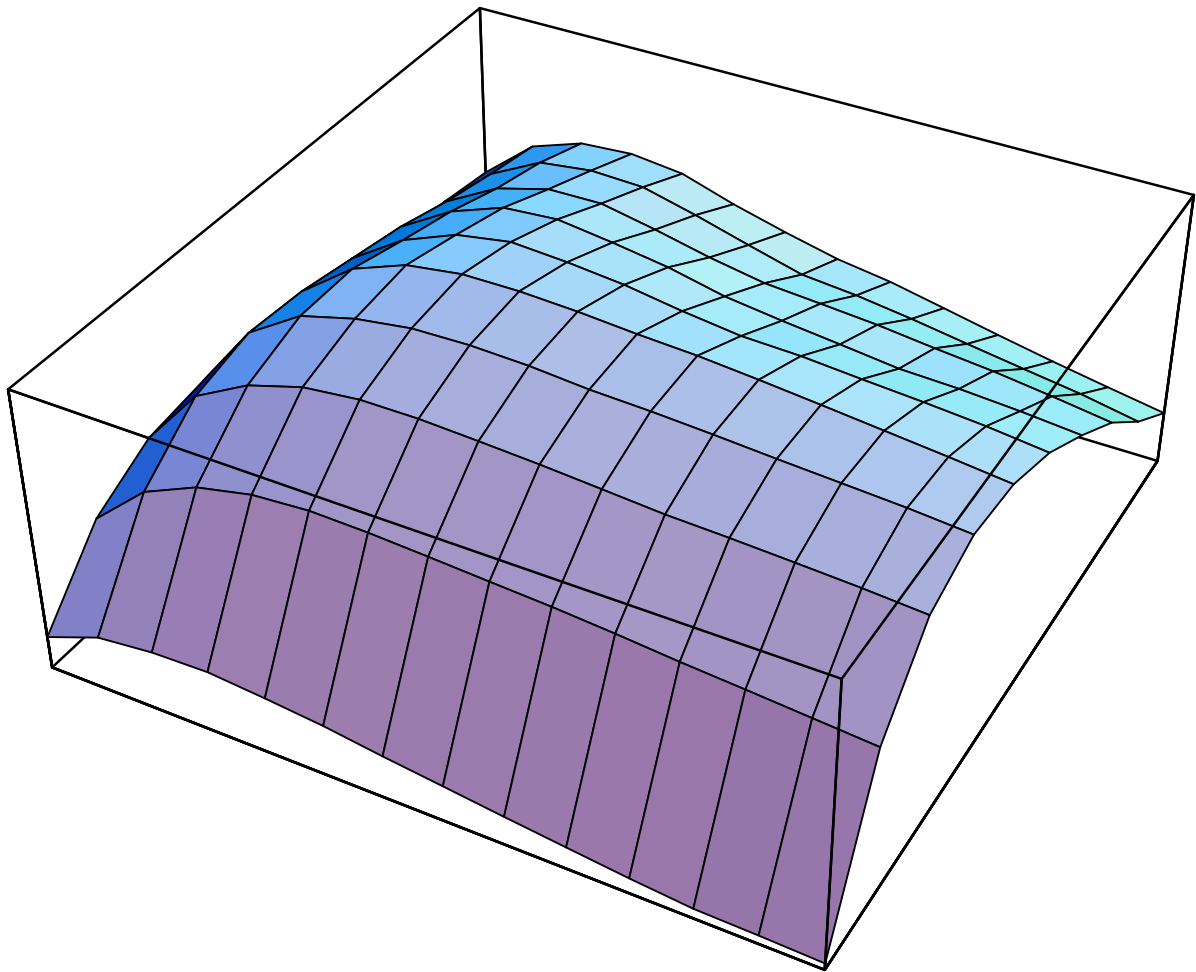


Fig. 13(a)

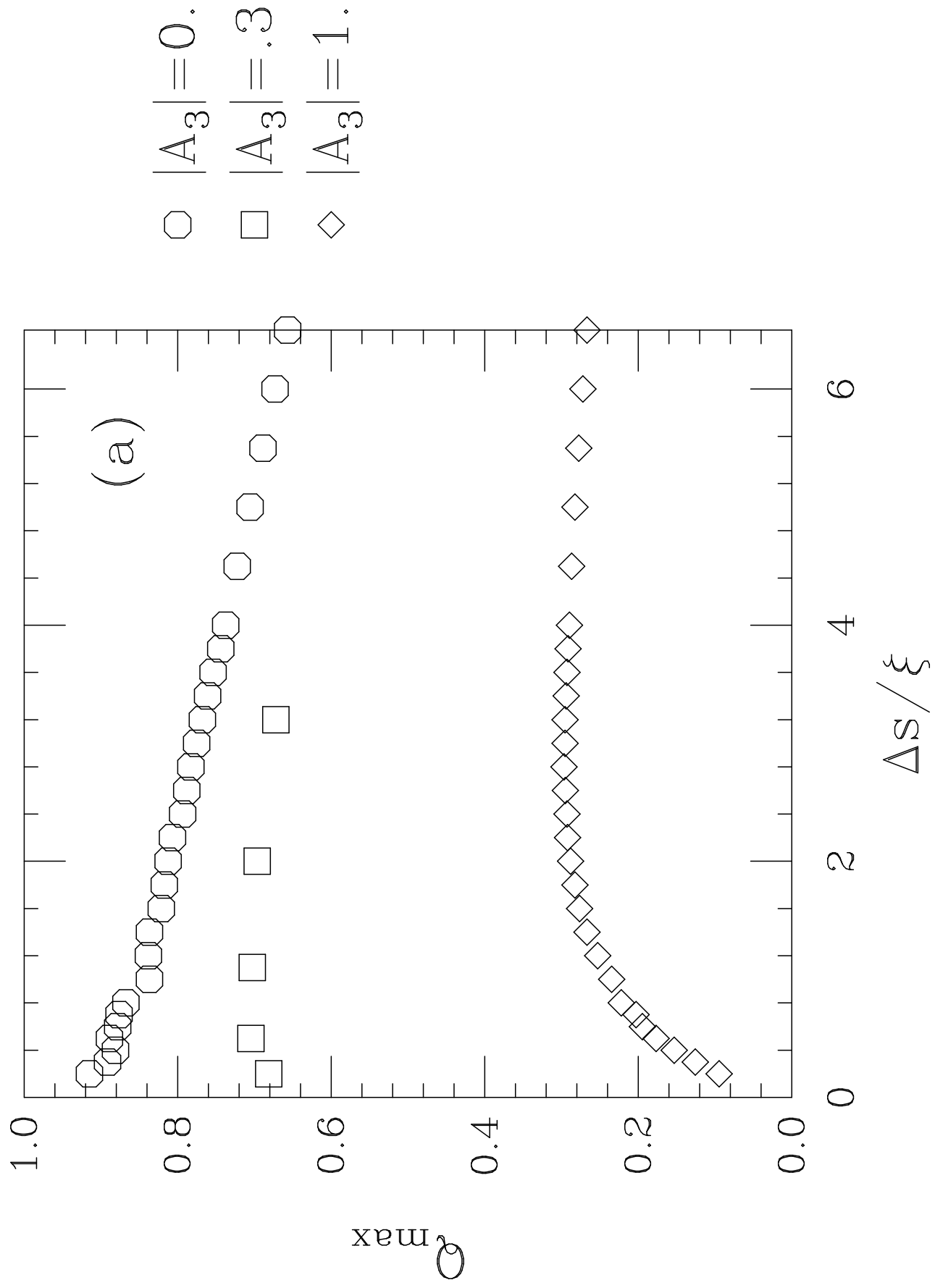


Fig. 13(b)

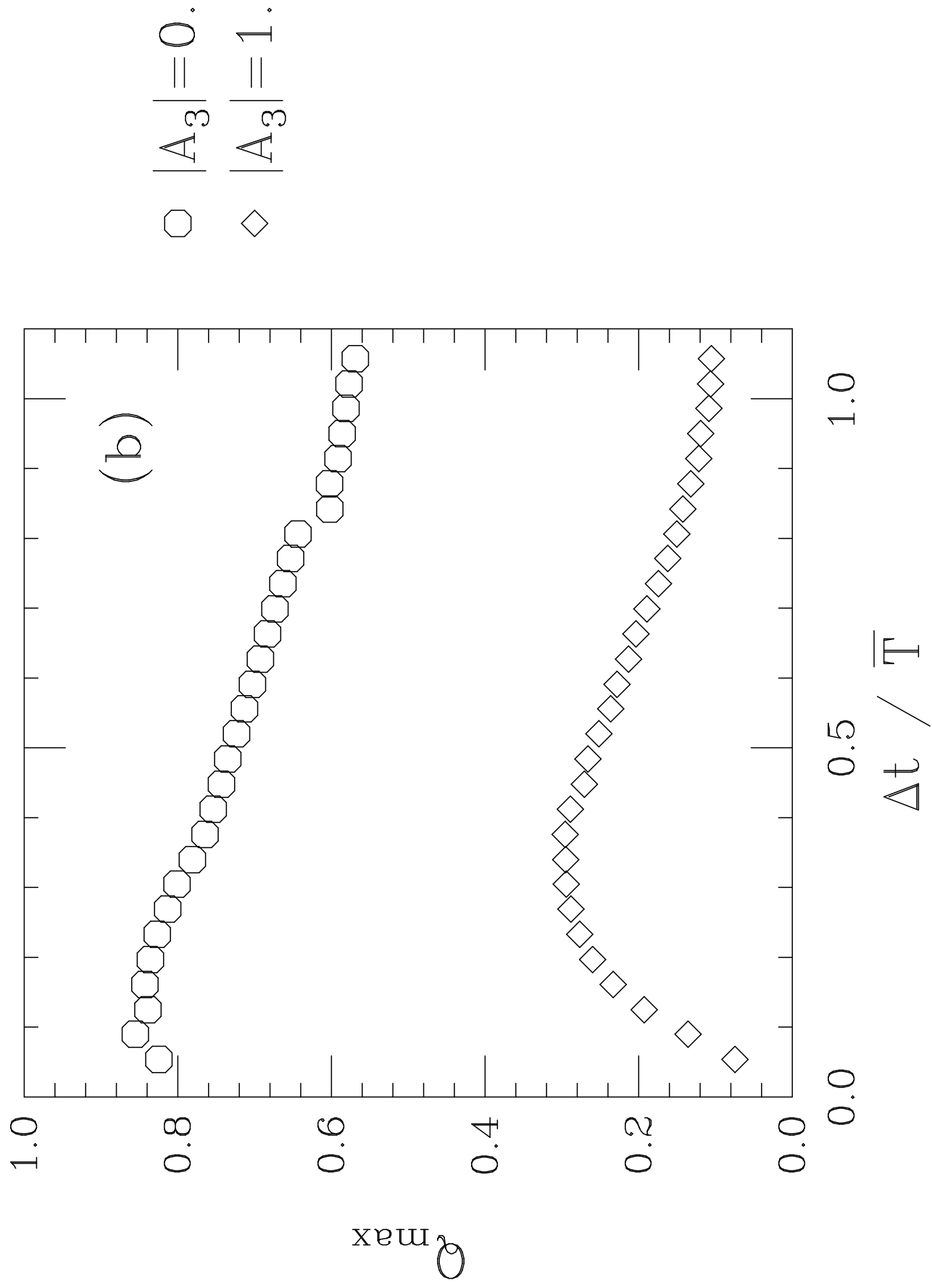


Fig. 14

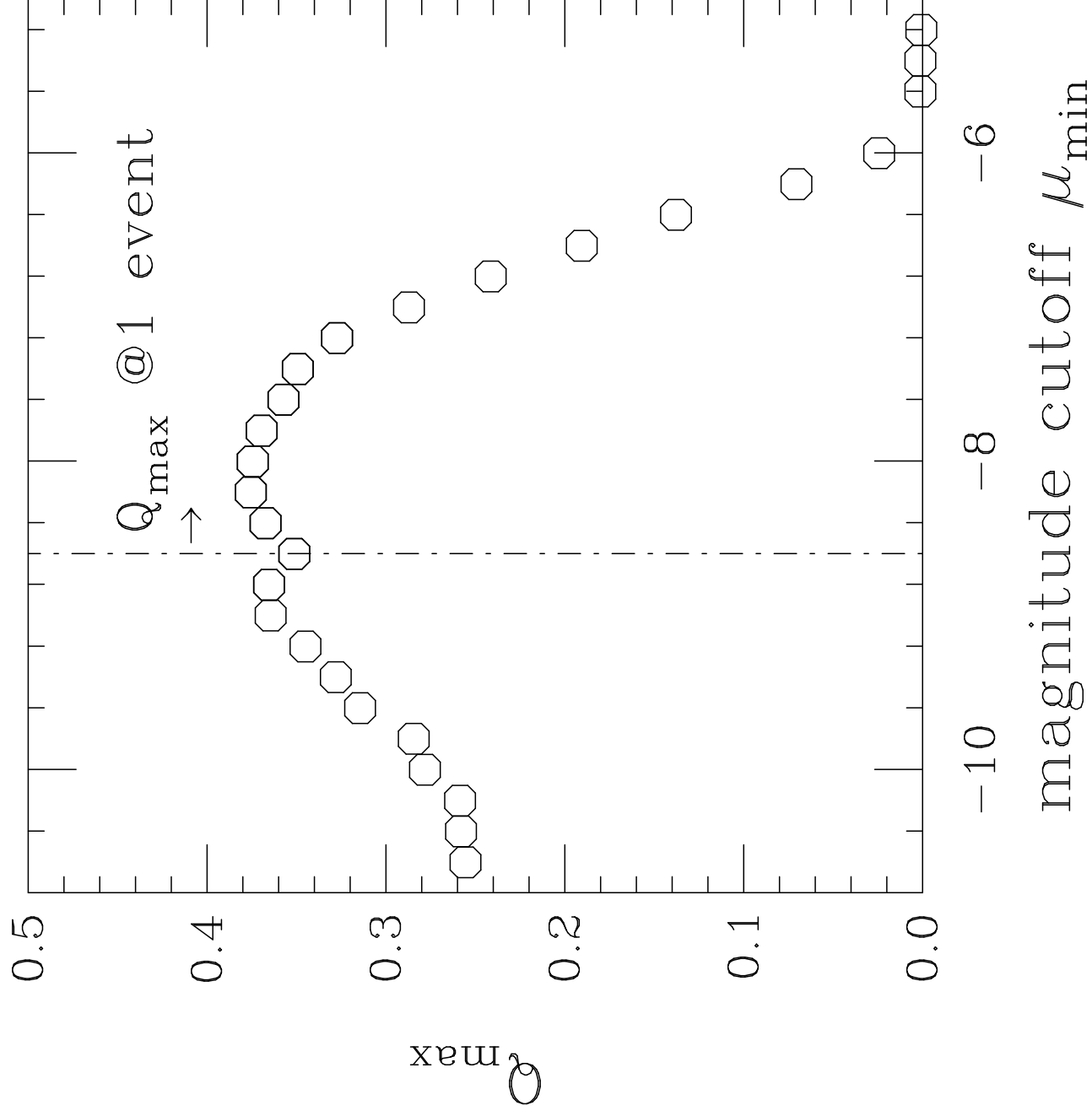




Fig. 15(a)

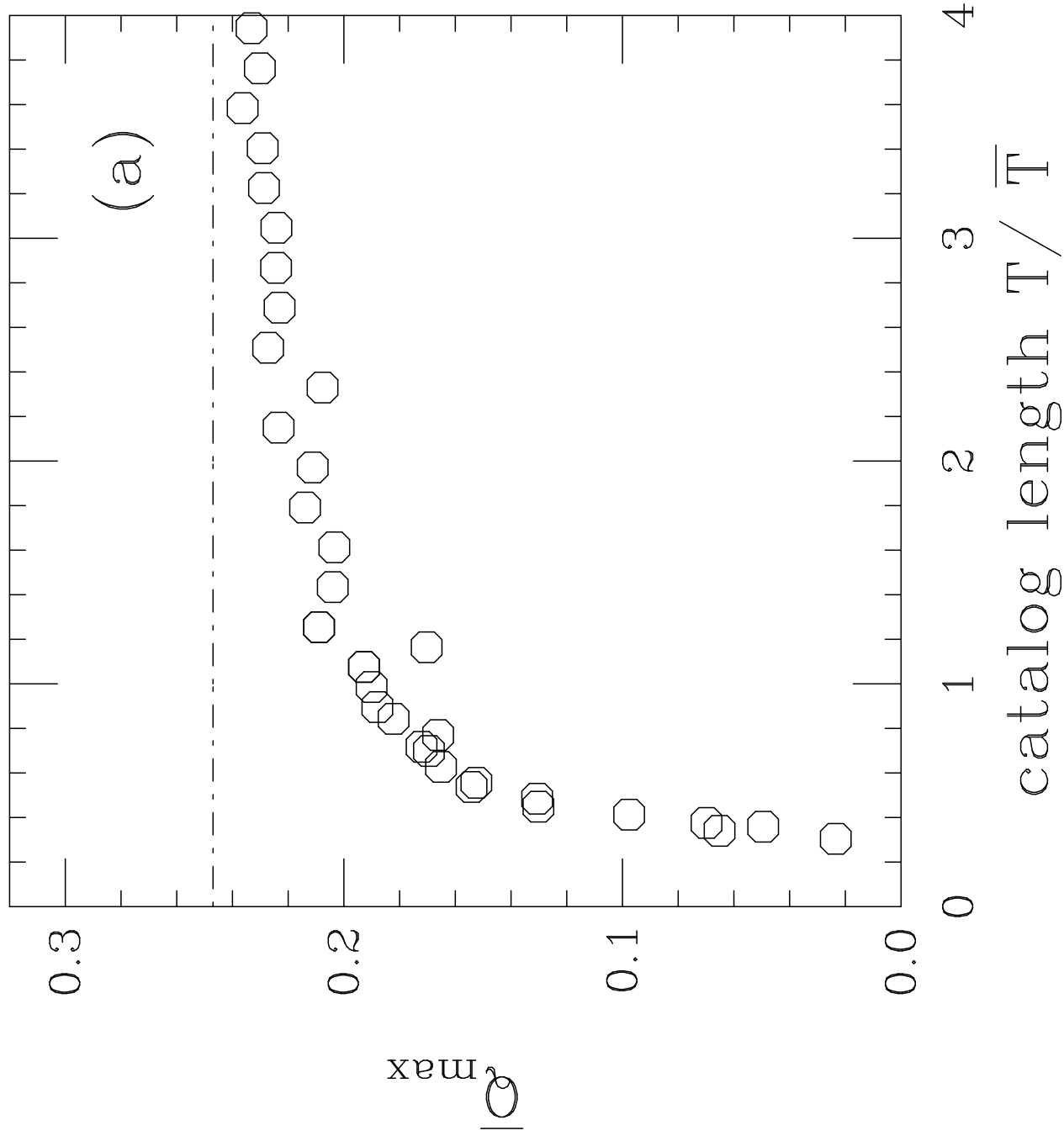


Fig. 15(b)

